1991), although very limited number of reports are available on the solid dispersion formulation of TL (Shibata et al., 2007). In general, amorphous substances are chemically and/or physically less stable than crystalline substances. Considering the poor photostability of TL in the solution state, crystalline solid dispersion (CSD) approach might be one of the viable formulation options for TL, possibly leading to high photostability and improved bioavailability, although the formulation has never been prepared and characterized.

The purpose of the present investigation was to develop novel oral formulation of TL for improving oral bioavailability and photostability. CSD formulation of TL (CSD/TL) was prepared with a wet-milling technique, followed by freeze-drying. Physicochemical properties of CSD/TL were characterized with emphasis on surface morphology, particle size distribution, crystallinity, thermal behavior, dissolution, and photostability. In photostability testing, photochemical properties of CSD/TL, crystalline TL, and amorphous SD formulation of TL (ASD/TL) were assessed for comparison purpose. Pharmacokinetic profiling of TL after oral administration of CSD/TL or crystalline TL in rats was made with use of ultra-performance liquid chromatography equipped with electrospray ionization mass spectrometry (UPLC/ESI-MS).

2. Materials and methods

2.1. Chemicals

TL (crystal) was supplied from Kissei Pharmaceutical Co., Ltd. (Nagano, Japan). Hydroxypropyl cellulose SL (HPC-SL) was supplied from Nippon Soda Co., Ltd. (Tokyo, Japan). Sodium dodecyl sulfate (SDS) and 1,4-dioxane were purchased from Wako Pure Chemical Industries, Ltd. (Osaka, Japan). All other chemicals were purchased from commercial sources.

2.2. Tranilast formulations

2.2.1. Crystalline solid dispersion (CSD/TL)

The wet-milled TL formulation was prepared with NanoMill®-01 system (Elan Drug Technologies, Dublin, Ireland). In brief, 882.0 mg of crystalline TL was weighed and added in a 100 ml stainless chamber. Polystyrene beads (46.7 g) with diameter of 0.5 mm were put into the chamber and 44.1 ml of 5 mg/ml HPC-SL solution with 0.2 mg/ml SDS was added. The TL colloidal suspension was micronized at 3600 rpm for 90 min with NanoMill®-01 system with cooling the chamber at 5 °C. After micronization with wet-milling process, the TL wet-milled suspension was collected and lyophilized with LyoStar II® freeze-dryer (SP Industries Inc., Warminster, PA, USA).

2.2.2. Amorphous solid dispersion (ASD/TL)

Crystalline TL (400 mg) and HPC-SL (1600 mg) were dissolved in 90% (v/v) 1,4-dioxane solution and frozen at −80 °C. The frozen mixture was lyophilized with LyoStar II® freeze-dryer (SP Industries Inc., Warminster, PA, USA). After drying, the sample was sieved with two different mesh sizes of sieves (2.0 and 1.0 mm).

2.2.3. Physical mixture (PM/TL)

TL (100 mg) and HPC-SL (400 mg) were added into a polyethylene tube and blended with a Turbula® Shaker-Mixer (Willy A. Bachofen AG Maschinenfabrik, Switzerland) at 30 rpm for 15 min.

2.3. Electron microscope

2.3.1. Scanning electron microscope (SEM)

Representative scanning electron microscopic images of TL samples were taken using a scanning electron microscope, VE-7800 (Keyence Corporation, Osaka, Japan), without Au or Pt coating. For the SEM observations, each sample was fixed on an aluminum sample holder using a double-side carbon tape.

2.3.2. Transmission electron microscope (TEM)

An aliquot (2 μl) of wet-milled TL suspension was placed on a carbon-coated Formvar 200 mesh nickel grid. The sample was allowed to stand for 15–30 s, and then any excess solution was removed by blotting. The samples were negatively stained with 2% (w/v) uranyl acetate and allowed to dry. The samples were then visualized under as H-7600 transmission electron microscope (Hitachi, Japan) operating at 75 kV.

2.4. Particle size analysis

2.4.1. Laser diffraction

Particle size of TL was measured by laser diffraction scattering method using a Microtrac HRA X-100 (Nikkiso Co., Ltd., Tokyo, Japan). For measurement, TL was suspended in distilled water. Particle size distribution was expressed as the volume median diameter and SPAN factor defined as $SPAN = (d_{90} - d_{10})/d_{50}$, where d_{10}, d_{50} and d_{90} are the particle diameters at 10%, 50% and 90% of the cumulative volume, respectively. A high SPAN value indicates a wide size distribution.

2.4.2. Dynamic light scattering (DLS)

Particle size of wet-milled TL was measured by dynamic light scattering method using a N5 submicron particle size analyzer (Beckman Coulter Inc., Brea, CA, USA). For measurement, one drop of TL suspension was diluted with ca. 4 ml distilled water and dispersed homogeneously. Mean diameter was calculated using a photon correlation from light scattering. All measurements were performed at 25 °C at a measurement angle of 90°. The size distribution, which was calculated by histogram analysis of scattering intensity, was evaluated at cumulative values of 10%, 50% and 90%.

2.5. X-ray powder diffraction (XRPD)

The powder X-ray diffraction pattern was collected with D8 Advance (Bruker AXS GmbH, Karlsruhe, Germany) with Cu Kα radiation generated at 40 mA and 35 kV. Data were obtained from 4° to 40° (2θ) at a step size of 0.014° and scanning speed of 4°/min.

2.6. Thermal analysis

Differential scanning calorimetry (DSC) was performed using a DSC Q1000 (TA instruments, New Castle, DE, USA). DSC thermograms were collected in an aluminum close-pan system using a sample weight of ca. 3 mg and a heating rate of 5 °C/min with nitrogen purge at 70 ml/min. The temperature axis was calibrated with indium (ca. 5 mg, 99.999% pure, onset at 156.6 °C).

2.7. Dissolution test

Dissolution tests were carried out for 60 min in 900 ml purified water with constant stirring of 50 rpm in a dissolution test apparatus DE-1S (Tokyo Rikakikai Co., Ltd., Tokyo, Japan) at 37 °C. One milligram of each TL sample was weighed to the dissolution vessel. Samples were collected at the indicated periods up to 60 min and centrifuged at 15,000 × g for 5 min. The supernatants were diluted with ethanol, and the amount of TL was determined by Waters Acquity UPLC system (Waters, Milford, MA, USA) that includes the binary solvent manager, sample manager, column compartment, and SQD connected with MassLynx software. An Acquity UPLC BEH C 18 column (particle size: 1.7 μm, column size: 2.1 mm × 50 mm;

Waters), also from Waters, was used, and column temperature was maintained at 50 °C. The samples were separated using a gradient mobile phase consisting of 5 mM ammonium acetate (A) and methanol (B) with the flow rate of 0.25 ml/min, and the retention time of TL was 1.7 min. The gradient condition of mobile phase was 0–0.5 min, 40% B; and 0.5–3.5 min, 40–65% B.

2.8. Photostability of tranilast formulations

2.8.1. Irradiation conditions

UV irradiation experiments were carried out using an Atlas Suntest CPS+ solar simulator (Atlas Material Technology LLC, Chicago, IL, USA) equipped with a xenon arc lamp (1500 W). UV special filter and window glass filter were installed to adapt the spectrum of the artificial light source to natural daylight. The irradiation test was carried out at 25 °C with an irradiance of 250 W/m^2. A reference sample under the protection of aluminum foil was examined under the same condition.

2.8.2. Photostability testing

For solid-state stability test, each TL formulation (2 mg) was weighed exactly and spread in 1.5 ml clear glass vial (12 mm × 32 mm, Shimadzu, Kyoto, Japan) over the whole bottom surface. For solution state stability study, 1 mg of crystalline TL was weighed in 1.5 ml clear glass vial and dissolved in 1 ml of dimethyl sulfoxide. TL formulations were set in the Suntest CPS+ solar simulator and irradiated with UVA/B light (0–450 kJ/m^2), and the remaining TL in the sample was determined by UPLC/ESI-MS, as described in Section 2.7.

2.9. In vivo experiments

2.9.1. Animals and drug administration

Male Sprague–Dawley rats (Japan SLC, Shizuoka, Japan), weighing 286 ± 42 g, were housed two per cage in the laboratory with free access to food and water, and maintained on a 12-h dark/light cycle in a room with controlled temperature (24 ± 1 °C) and humidity (55 ± 5%). All the procedures used in the present study were conducted according to the guidelines approved by the Institutional Animal Care and Ethical Committee of University of Shizuoka. For oral administration, each TL formulation was suspended in saline. Rats were fasted for approximately 24 h before drug administration, and received orally TL formulations (10 mg-TL/kg body weight). For intravenous injection, 0.3 mg of TL was suspended in 1.0 ml of PBS, and the TL suspension was sonicated for 30 min in ultra sonic cleaner US-1R (As One, Osaka, Japan) for complete dissolution. The TL solution was injected intravenously in rats (0.5 mg/kg body weight).

2.9.2. Serum concentration of tranilast

Blood samples (400 μl) were collected from the tail vein at the indicated periods after oral administration of TL or TL formulation. Each blood sample (400 μl) was centrifuged at 10,000 × *g* to prepare serum samples. The serum samples were kept frozen at below −20 °C until they were analyzed. TL concentrations in serum were estimated by UPLC/ESI-MS. In brief, 100 μl of methanol was added to 50 μl of serum sample, and the solution was centrifuged at 3000 rpm for 10 min. The supernatant was filtrated through the 0.2-μm filter, and then the filtrate was analyzed by UPLC/ESI-MS, as described in Section 2.7.

2.10. Statistical analysis

For statistical comparisons, a one-way analysis of variance (ANOVA) with the pairwise comparison by Fisher's least significant difference procedure was used. A P value of <0.05 was considered significant for all analyses.

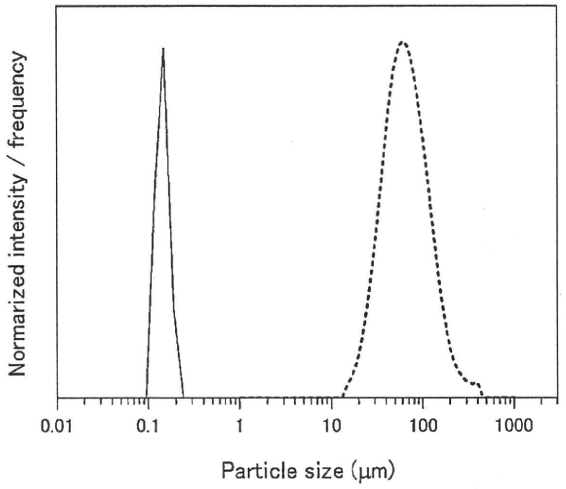

Fig. 1. Size distributions of TL and wet-milled TL suspension. Particle sizes of TL and wet-milled TL suspension were determined by laser diffraction and dynamic light scattering method, respectively. Solid line, TL wet-milled suspension; and dashed line, TL.

3. Results and discussion

3.1. Preparation of tranilast-loaded solid dispersion

Initially, crystalline TL, suspended in HPC-SL solution containing 0.2% SDS, was wet-milled for reduction of particle size, with an overall yield of ca. 45%. Particle sizes of TL and the wet-milled TL suspension were evaluated by laser diffraction and DLS analyses, respectively (Fig. 1). The mean particle diameter of TL was calculated to be 61.4 μm with SPAN factor of 2.6. According to DLS data on wet-milled TL suspension, the mean particle diameter of TL was reduced from 61.4 μm to 122.2 nm, and SPAN factor was reduced to 0.6 by wet-milling process. These data indicated that milled TL particles seemed to be homogeneous with a narrow particle size distribution. The suspension of wet-milled TL was freeze-dried to prepare SD formulation, and the resultant formulation appeared as a thin and flaky material according to SEM observations (Fig. 2). Interestingly, TEM image on the water-dispersed SD formulation demonstrated that wet-milled TL particles could be re-dispersed into water without forming any large aggregates (Fig. 2C).

Previous works demonstrated that TL had several anhydrate and hydrate forms (Kawashima et al., 1991; Vogt et al., 2005). To clarify the polymorphic transformation of TL during the wet-milling and subsequent freeze-drying process, XRPD analyses on crystalline TL and wet-milled formulation of TL were carried out (Fig. 3A). The XRPD data on crystalline TL showed a characteristic peak at 24.9°, and its diffraction pattern was almost identical to that of the most stable anhydrous crystalline form reported previously (Kawashima et al., 1991). Wet-milled formulation of TL, even after freeze-drying, exhibited the similar XRPD patterns of TL and the physical mixture of TL and HPC-SL (PM/TL), suggesting that any polymorphic transformation or hydration might not occur during the wet-milling and subsequent freeze-drying process. For characterizing molecular property of TL formulation in more detail, thermal behaviors were also clarified with use of DSC (Fig. 3B). Generally, thermal behaviors of drug formulations are also important in pharmaceutical technologies, since the obtained information such as melting, recrystallization, decomposition, or a

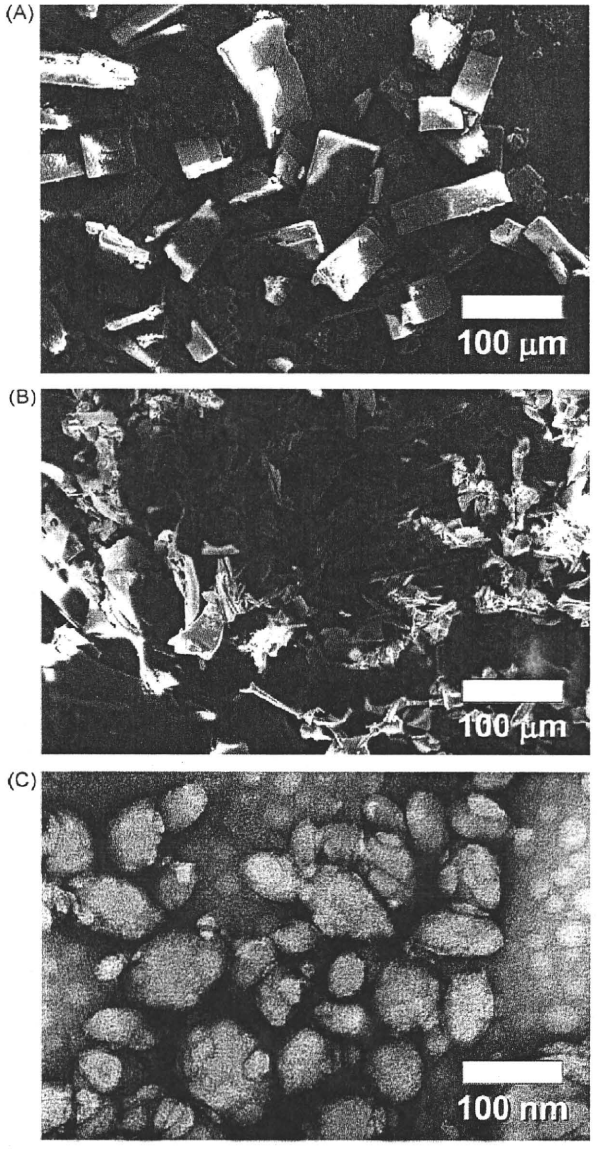

Fig. 2. Morphological observations of TL and CSD/TL. Scanning electron microscopic images of TL (A) and CSD/TL (B). Transmission electron microscopic image of dispersed nanocrystals (C).

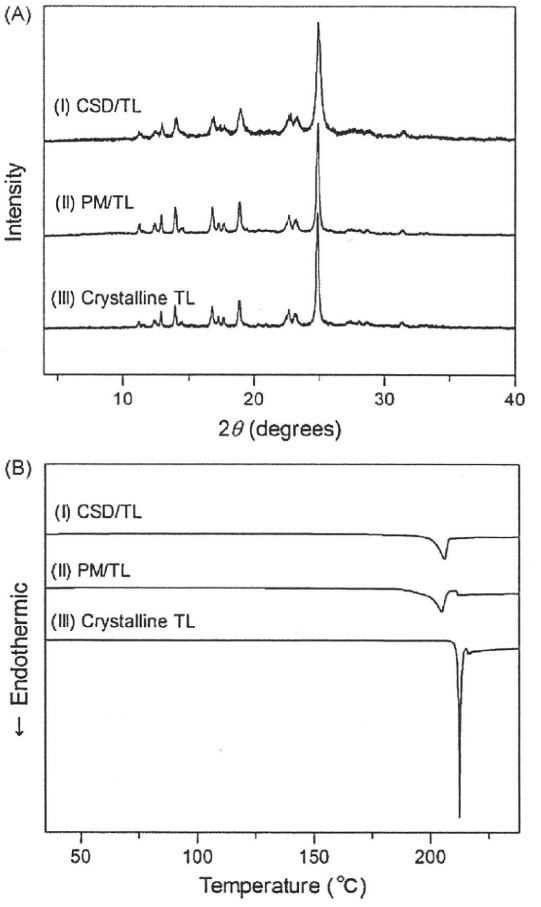

Fig. 3. Physicochemical characterization of TL samples, including (I) CSD/TL, (II) PM/TL, and (III) crystalline TL. (A) Powder X-ray diffraction patterns and (B) DSC thermograms.

change in heat capacity could help to ascertain the physicochemical status of the entrapped drug inside the excipient. Crystalline TL showed a sharp melting endothermic peak at 212 °C (Fig. 3B-III), whereas the endothermic peak of CSD/TL became broad and shifted to lower temperature as compared to crystalline TL (Fig. 3B-I). Thermal behavior of wet-milled formulation of TL was similar to that of PM/TL (Fig. 3B-II), proposing that transition of the thermal behavior on wet-milled formulation was due to the co-existence of the excipients. Thermal analyses indicated that any physicochemical transition of TL did not occur during the formulation processes, supporting the results from XRPD analyses.

On the basis of SEM observation and XRPD analyses, micronized TL might be homogeneously dispersed in HPC-SL as fine crystalline particles. Basically, solid dispersion can be defined as a distribution of active ingredients in molecular, amorphous, and/or microcrystalline forms surrounded by inert carriers (Chiou and Riegelman, 1971). Herein, the newly developed TL formulation in the present study can be identified as a nano-crystalline solid dispersion of TL (CSD/TL).

3.2. Dissolution behaviors of tranilast formulations

It is well-established that, for poorly water-soluble drugs, especially class II drugs in biopharmaceutic classification system, improvement of the drug solubility sometimes result in the marked increase of the oral bioavailability (Amidon et al., 1995). To clarify the dissolution behavior of TL formulation, the dissolution tests on crystalline TL, CSD/TL and PM/TL were carried out up to 60 min in water (Fig. 4). Crystalline TL and PM/TL exhibited poor dissolution/dispersion rates in water, and amounts of dissolved TL from the TL and PM/TL at 60 min was found to be ca. 10% and 19%, respectively. Upon these data, slight improvement in the dissolution properties of PM/TL suggested that HPC-SL itself might act as a weak solubilizer in the present formulations, contributing to the limited increase in drug dissolution, as well as prevention of drug aggregation. In contrast, CSD/TL showed the accelerated dissolution behavior as evidenced by release of ca. 97% TL from CSD/TL at 10 min. According to Nernst–Brunner and Levich modification of the Noyes Whitney dissolution model equations, the dissolution rate of a drug is proportional to its effective surface area (Dressman et al., 1998; Horter and Dressman, 2001). As defined by the Prandtl equation, the decrease of diffusion layer thickness by reducing particle size, particularly down to <5 μm, would result in the accel-

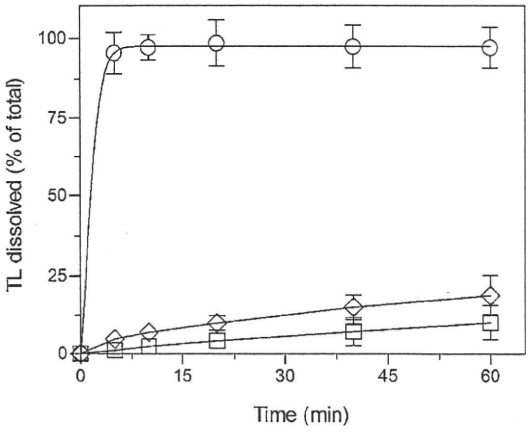

Fig. 4. Dissolution profiles of TL formulations in water. (○) CSD/TL; (□) TL; and (◊) PM/TL. Each bar represents mean ± SE of 3 independent experiments.

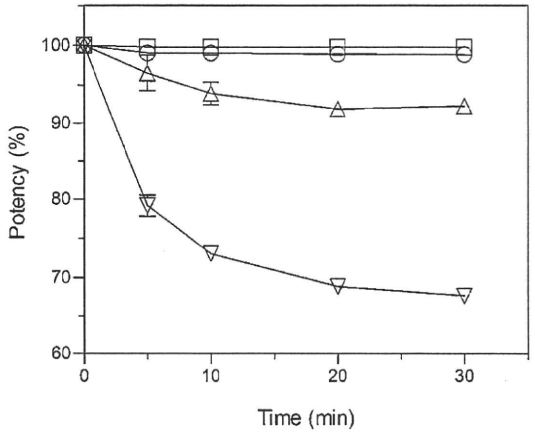

Fig. 5. Photodegradation profile of TL formulations. Each TL sample was exposed to UVA/UVB (250 W/m^2) for indicated periods, and purity was assessed by UPLC/ESI-MS. (○) CSD/TL; (△) ASD/TL; (□) TL; and (▽) TL solution.

erated dissolution (Mosharraf and Nystrom, 1999). The enhanced dissolution rate, observed in CSD/TL, would be attributed to the increase of effective surface area and saturation solubility, and the decrease of diffusion layer thickness by particle size reduction to sub-micron range. Generally, nanocrystal formulations of poorly water-soluble drug can lead to marked improvement in the dissolution rate, and the improved dissolution behavior often resulted in an increase in the oral bioavailability (Jinno et al., 2006; Kondo et al., 1993). Based on the dissolution profiles, as well as physicochemical characteristics of novel TL formulations developed, CSD formulation might be suitable for oral use because of the improved dissolution property in water.

3.3. Photochemical stability of tranilast formulations

As previously reported (Hori et al., 1999), TL in the solution state was photochemically unstable, yielding two major photoproducts such as *cis*-isomer and TL dimer. Since these photodegradants were less effective than TL in treatment of dermal inflammation, improvement of photostability would be one of key considerations for development of the potent TL formulations. In the present investigation, photostability test employing a solar simulator was carried out on TL solution, crystalline TL, and SD formulations of nanocrystal TL (CSD/TL) and high-energy amorphous TL (ASD/TL) (Fig. 5). Degradation kinetics was calculated according to the following equation: $\ln A = \ln A_0 - kt$, where A is the remaining peak area of TL, t is the time (min) and k is the slope (degradation constant). Exposure of TL solution to the simulated sunlight (250 W/m^2) for the indicated periods resulted in marked degradation of TL, degradation constant of which was calculated to be 3.1×10^{-2} min^{-1}. TL solution exhibited 32% decrease of potency after UV irradiation, suggesting that liquid formulation approach, e.g. co-solvents and emulsions, might not be suitable for TL. On the contrary, crystalline TL was found to be photochemically stable with a degradation rate constant of 2.4×10^{-4} min^{-1}. These observations could be consistent with our previous observation, demonstrating that photodegradation of crystalline dihydropyridine derivative was much slower than that in the solution state (Onoue et al., 2008). To improve oral bioavailability of poorly water-soluble drugs, high-energy amorphous SD approach is frequently used (Vasconcelos et al., 2007). In the present study, ASD/TL was prepared by freeze-drying technique, and its photostability was also compared to CSD/TL in the solid state. Irradiated ASD/TL exhibited slight photodegradation with a degradation rate constant of 6.3×10^{-3} min^{-1}, whereas CSD/TL was found to be photochemically stable as evidenced by low degradation constant (9.7×10^{-4} min^{-1}). Generally, crystalline chemicals tend to be more stable than the amorphous form, and this could be a part of reasons for differences in photostability between ASD/TL and CSD/TL. According to the photodegradation kinetics calculated, the order of photostability was as follows: TL > CSD/TL > ASD/TL ≫ TL solution. These findings suggested that crystalline solid dispersion approach would be more suitable for TL than liquid or amorphous formulation from photochemical point of view.

3.4. Pharmacokinetic profiling of tranilast formulations

The observations on the improved dissolution properties of CSD/TL prompted us to clarify the possible improvement in absorption of TL, so the pharmacokinetic behaviors of TL formulations were assessed in rats. Fig. 6 shows the blood concentration–time profiles of TL in rats after oral administration of CSD/TL and TL (10 mg-TL/kg), and relevant pharmacokinetic parameters including C_{max}, T_{max}, $T_{1/2}$, AUC_{0-inf}, and absolute bioavailability are listed in Table 1. Serum TL levels in the blood were found to be very low when TL was administered orally, and the C_{max} and AUC_{0-inf} values were 0.1 μg/ml and 0.8 μg/ml h, respectively. On the contrary,

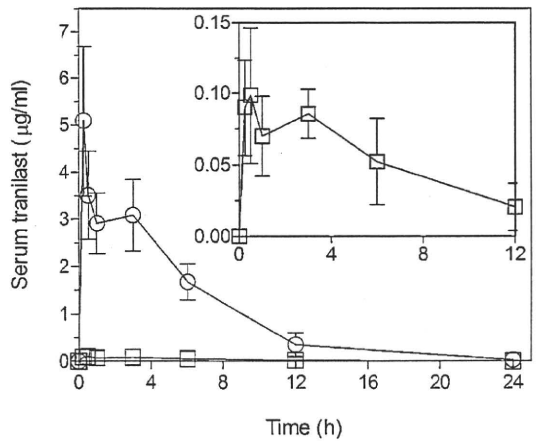

Fig. 6. Serum TL concentrations in rats after oral administration of TL and TL formulations. (○) CSD/TL; and (□)TL (10 mg-TL/kg body weight of rat as a single dose). The inset highlights the concentration values obtained after oral administration of TL. Data represent mean ± SE of 4–5 experiments.

Table 1
Pharmacokinetic parameters of tranilast formulations following oral administration.

Formulations	C_{max} (μg/ml)	T_{max} (h)	$T_{1/2}$ (h)	AUC_{0-inf} (μg/ml h)	BA (%)
Crystalline TL (10 mg/kg)	0.1 ± 0.0	1.8 ± 0.7	2.9 ± 0.7	0.8 ± 0.4	1.2
CSD/TL (10 mg-TL/kg)	6.0 ± 1.3**	2.5 ± 1.1	2.2 ± 0.5	24.8 ± 2.4**	37.7

C_{max}: maximum concentration; T_{max}: time to maximum concentration; $T_{1/2}$: half-life; and AUC_{0-inf}: area under the curve of serum concentration vs time from $t=0$ to $t=\infty$ after administration. BA: absolute bioavailability. Values are expressed as means ± SE from 4 to 5 experiments.
** $P<0.01$ with respect to crystalline TL.

CSD/TL showed improved pharmacokinetic behavior as compared to TL. Oral administration of CSD/TL resulted in rapid elevation of TL blood levels up to C_{max} 6.0 μg/ml, and the AUC_{0-inf} value was calculated to be 24.8 μg/ml h. Thus, there appeared to be ca. 60- and 31-fold enhancement in C_{max} and AUC_{0-inf} of TL with the use of wet-milling technology. On the basis of AUC value of intravenously administered TL (0.5 mg/kg, data not shown), absolute bioavailabilities of TL and CSD/TL were calculated to be 1.2% and 37.7%, respectively. These findings were relatively consistent with the results from dissolution test, demonstrating the accelerated dissolution behavior of CSD/TL. Upon these findings, taken together with physicochemical properties and dissolution profiles, CSD approaches would be effective for developing the water-soluble formulation of TL with high photostability.

Currently, TL is administered orally at a dose of 300 mg/day in Japan for the clinical treatment of several inflammatory diseases, however TL at high dose sometimes cause gastrointestinal tract disturbance (Tamai et al., 1999). Because of 32-fold higher absolute bioavailability of CSD/TL compared with TL, CSD approach might lead to a considerable reduction of oral TL dose and a prevention of undesired side effects in gastrointestinal tract. Furthermore, the enhanced oral bioavailability of TL by CSD strategy could be advantageous for new clinical application of TL, that has been received attention in recent years, e.g. hepatic fibrosis (Ikeda et al., 1996; Uno et al., 2008), pulmonary fibrosis (Mori et al., 1991, 1995), and cancer (Izumi et al., 2009; Nie et al., 1997; Noguchi et al., 2003).

4. Conclusions

In the present study, nanocrystal TL-loaded SD formulation was prepared with aim of high photostability and enhanced oral bioavailability. There was marked improvement in dissolution behavior of CSD/TL as compared to TL and PM/TL. Although both solution and amorphous formulation of TL were found to be photodegradable, high photochemical stability was observed in CSD/TL and TL. Pharmacokinetic data on CSD/TL was indicative of high systemic exposure with increase of C_{max} and AUC_{0-inf} by ca. 60- and 31-fold for TL, respectively. Upon these observations, taken together with physicochemical properties, CSD approach would be efficacious to enhance bioavailability of TL with high photostability, possibly providing advantages for clinical treatment of several chronic inflammatory diseases.

Acknowledgements

Authors are grateful to Kissei Pharmaceutical Co., Ltd. (Nagano, Japan) for kindly providing tranilast. This work was supported in part by a Grant-in-Aid for Young Scientists (B) (No. 20790103; S. Onoue) from the Ministry of Education, Culture, Sports, Science and Technology, and Research and Development Projects for Application in Promoting New Policy of Agriculture Forestry and Fisheries from the Ministry of Agriculture, Forestry and Fisheries.

References

Amidon, G.L., Lennernas, H., Shah, V.P., Crison, J.R., 1995. A theoretical basis for a biopharmaceutic drug classification: the correlation of in vitro drug product dissolution and in vivo bioavailability. Pharm. Res. 12, 413–420.
Berge, S.M., Bighley, L.D., Monkhouse, D.C., 1977. Pharmaceutical salts. J. Pharm. Sci. 66, 1–19.
Brewster, M.E., Loftsson, T., 2007. Cyclodextrins as pharmaceutical solubilizers. Adv. Drug Deliv. Rev. 59, 645–666.
Chiou, W.L., Riegelman, S., 1971. Pharmaceutical applications of solid dispersion systems. J. Pharm. Sci. 60, 1281–1302.
Dressman, J.B., Amidon, G.L., Reppas, C., Shah, V.P., 1998. Dissolution testing as a prognostic tool for oral drug absorption: immediate release dosage forms. Pharm. Res. 15, 11–22.
Hori, N., Fujii, M., Ikegami, K., Momose, D., Saito, N., Matsumoto, M., 1999. Effect of UV-absorbing agents on photodegradation of tranilast in oily gels. Chem. Pharm. Bull. (Tokyo) 47, 1713–1716.
Horter, D., Dressman, J.B., 2001. Influence of physicochemical properties on dissolution of drugs in the gastrointestinal tract. Adv. Drug Deliv. Rev. 46, 75–87.
Ikeda, H., Inao, M., Fujiwara, K., 1996. Inhibitory effect of tranilast on activation and transforming growth factor beta 1 expression in cultured rat stellate cells. Biochem. Biophys. Res. Commun. 227, 322–327.
Izumi, K., Mizokami, A., Li, Y.Q., Narimoto, K., Sugimoto, K., Kadono, Y., Kitagawa, Y., Konaka, H., Koh, E., Keller, E.T., Namiki, M., 2009. Tranilast inhibits hormone refractory prostate cancer cell proliferation and suppresses transforming growth factor beta1-associated osteoblastic changes. Prostate 69, 1222–1234.
Jinno, J., Kamada, N., Miyake, M., Yamada, K., Mukai, T., Odomi, M., Toguchi, H., Liversidge, G.G., Higaki, K., Kimura, T., 2006. Effect of particle size reduction on dissolution and oral absorption of a poorly water-soluble drug, cilostazol, in beagle dogs. J. Control. Release 111, 56–64.
Kawashima, Y., Niwa, T., Takeuchi, H., Hino, T., Itoh, Y., 1992. Hollow microspheres for use as a floating controlled drug delivery system in the stomach. J. Pharm. Sci. 81, 135–140.
Kawashima, Y., Niwa, T., Takeuchi, H., Hino, T., Itoh, Y., Furuyama, S., 1991. Characterization of polymorphs of tranilast anhydrate and tranilast monohydrate when crystallized by two solvent change spherical crystallization techniques. J. Pharm. Sci. 80, 472–478.
Koda, A., Nagai, H., Watanabe, S., Yanagihara, Y., Sakamoto, K., 1976. Inhibition of hypersensitivity reactions by a new drug, N(3′,4′-dimethoxycinnamoyl) anthranilic acid (N-5′). J. Allergy Clin. Immunol. 57, 396–407.
Kondo, N., Iwao, T., Masuda, H., Yamanouchi, K., Ishihara, Y., Yamada, N., Haga, T., Ogawa, Y., Yokoyama, K., 1993. Improved oral absorption of a poorly water-soluble drug, HO-221, by wet-bead milling producing particles in submicron region. Chem. Pharm. Bull. (Tokyo) 41, 737–740.
Mori, H., Kawada, K., Zhang, P., Uesugi, Y., Sakamoto, O., Koda, A., 1991. Bleomycin-induced pulmonary fibrosis in genetically mast cell-deficient WBB6F1-W/Wv mice and mechanism of the suppressive effect of tranilast, an antiallergic drug inhibiting mediator release from mast cells, on fibrosis. Int. Arch. Allergy Appl. Immunol. 95, 195–201.
Mori, H., Tanaka, H., Kawada, K., Nagai, H., Koda, A., 1995. Suppressive effects of tranilast on pulmonary fibrosis and activation of alveolar macrophages in mice treated with bleomycin: role of alveolar macrophages in the fibrosis. Jpn. J. Pharmacol. 67, 279–289.
Mosharraf, M., Nystrom, C., 1999. The effect of dry mixing on the apparent solubility of hydrophobic, sparingly soluble drugs. Eur. J. Pharm. Sci. 9, 145–156.
Nie, L., Oishi, Y., Doi, I., Shibata, H., Kojima, I., 1997. Inhibition of proliferation of MCF-7 breast cancer cells by a blocker of Ca(2+)-permeable channel. Cell Calcium 22, 75–82.
Noguchi, N., Kawashiri, S., Tanaka, A., Kato, K., Nakaya, H., 2003. Effects of fibroblast growth inhibitor on proliferation and metastasis of oral squamous cell carcinoma. Oral Oncol. 39, 240–247.
Onoue, S., Igarashi, N., Yamauchi, Y., Murase, N., Zhou, Y., Kojima, T., Yamada, S., Tsuda, Y., 2008. In vitro phototoxicity of dihydropyridine derivatives: a photochemical and photobiological study. Eur. J. Pharm. Sci. 33, 262–270.
Onoue, S., Sato, H., Kawabata, Y., Mizumoto, T., Hashimoto, N., Yamada, S., 2009. In vitro and in vivo characterization on amorphous solid dispersion of cyclosporine A for inhalation therapy. J. Control. Release 138, 16–23.
Serajuddin, A.T., 2007. Salt formation to improve drug solubility. Adv. Drug Deliv. Rev. 59, 603–616.
Shibata, Y., Fujii, M., Kokudai, M., Noda, S., Okada, H., Kondoh, M., Watanabe, Y., 2007. Effect of characteristics of compounds on maintenance of an

amorphous state in solid dispersion with crospovidone. J. Pharm. Sci. 96, 1537–1547.
Suzawa, H., Kikuchi, S., Arai, N., Koda, A., 1992a. The mechanism involved in the inhibitory action of tranilast on collagen biosynthesis of keloid fibroblasts. Jpn. J. Pharmacol. 60, 91–96.
Suzawa, H., Kikuchi, S., Ichikawa, K., Koda, A., 1992b. Inhibitory action of tranilast, an anti-allergic drug, on the release of cytokines and PGE2 from human monocytes–macrophages. Jpn. J. Pharmacol. 60, 85–90.
Talegaonkar, S., Azeem, A., Ahmad, F.J., Khar, R.K., Pathan, S.A., Khan, Z.I., 2008. Microemulsions: a novel approach to enhanced drug delivery. Recent Pat. Drug Deliv. Formul. 2, 238–257.
Tamai, H., Katoh, O., Suzuki, S., Fujii, K., Aizawa, T., Takase, S., Kurogane, H., Nishikawa, H., Sone, T., Sakai, K., Suzuki, T., 1999. Impact of tranilast on restenosis after coronary angioplasty: tranilast restenosis following angioplasty trial (TREAT). Am. Heart J. 138, 968–975.
The Society of Japanese Pharmacopoeia, 2002. Tranilast. In: Japanese Orange Books No. 12 (Approved drug products with therapeutic equivalence evaluations). Yakuji Nippo Ltd., Tokyo, p. 171.
Uno, M., Kurita, S., Misu, H., Ando, H., Ota, T., Matsuzawa-Nagata, N., Kita, Y., Nabemoto, S., Akahori, H., Zen, Y., Nakanuma, Y., Kaneko, S., Takamura, T., 2008. Tranilast, an antifibrogenic agent, ameliorates a dietary rat model of nonalcoholic steatohepatitis. Hepatology 48, 109–118.
Vasconcelos, T., Sarmento, B., Costa, P., 2007. Solid dispersions as strategy to improve oral bioavailability of poor water soluble drugs. Drug Discov. Today 12, 1068–1075.
Vogt, F.G., Cohen, D.E., Bowman, J.D., Spoors, G.P., Zuber, G.E., Trescher, G.A., Dell'orco, P.C., Katrincic, L.M., Debrosse, C.W., Curtis Haltiwanger, R., 2005. Structural analysis of polymorphism and solvation in tranilast. J. Pharm. Sci. 94, 651–665.

Pharm Res (2010) 27:1610–1619
DOI 10.1007/s11095-010-0161-3

RESEARCH PAPER

High-Throughput Screening System for Identifying Phototoxic Potential of Drug Candidates Based on Derivatives of Reactive Oxygen Metabolites

Satomi Onoue • Masanori Ochi • Graham Gandy • Yoshiki Seto • Naoko Igarashi • Yukinori Yamauchi • Shizuo Yamada

Received: 11 January 2010 / Accepted: 15 April 2010 / Published online: 27 April 2010

ABSTRACT

Purpose The present study aimed to develop a high-throughput screening strategy for predicting the phototoxic potential of pharmaceutical substances, using a derivatives-of-reactive-oxygen-metabolites (D-ROM) assay.

Methods The assay conditions of the D-ROM assay were optimized with a focus on screening run time, sensitivity, solvent system, and reproducibility. The phototoxic potentials of 25 model compounds were assessed by the D-ROM assay, as well as by other screening systems for comparison, including the reactive oxygen species (ROS) assay, the DNA-photocleavage assay, and the 3T3 neutral red uptake phototoxicity test (3T3 NRU PT).

Results Some phototoxic drugs tended to yield D-ROM when exposed to simulated sunlight (250 W/m^2), whereas D-ROM generation was negligible for non-phototoxic chemicals. Compared with the ROS assay, the assay procedure for the D-ROM assay was highly simplified with a marked reduction in screening run time. Comparative experiments also demonstrated that D-ROM data were related to the outcomes of the DNA-photocleavage assay and the 3T3 NRU PT, with prediction accuracies of 76 and 72%, respectively.

Conclusion The D-ROM assay has potential for identifying the phototoxic potential of a large number of new drugs as a 1st screening system in the early stages of drug discovery.

KEY WORDS 3T3 neutral red uptake phototoxicity test · derivatives of reactive oxygen metabolites · photogenotoxicity · phototoxicity · reactive oxygen species

ABBREVIATIONS

3T3 NRU PT	3T3 neutral red uptake phototoxicity test
5-FU	5-fluorouracil
8-MOP	8-methoxypsoralen
AFM	atomic force microscopy
AGE	agarose gel electrophoresis
CD	circular dichroism
DEPPD	*N,N*-diethyl-*p*-phenylenediamine
DMEM	Dulbecco's Modified Eagle Medium
D-ROM	derivatives of reactive oxygen metabolites
EBSS	Earle's Balanced Salt Solution
EtBr	ethidium bromide
ECVAM	Europe Center for the Validation of Alternative Methods
OC	open circular
OECD	Organisation for Economic Co-operation and Development
PIF	photoirritation factor
ROS	reactive oxygen species
SC	supercoiled

S. Onoue (✉) · M. Ochi · Y. Seto · S. Yamada
Department of Pharmacokinetics and Pharmacodynamics and Global Center of Excellence (COE) Program
School of Pharmaceutical Sciences, University of Shizuoka
52-1 Yada
Suruga-ku, Shizuoka 422-8526, Japan
e-mail: onoue@u-shizuoka-ken.ac.jp

G. Gandy
Drug Safety Research and Development
Pfizer Global Research and Development
Ramsgate Rd.
Sandwich CT13 9NJ, UK

N. Igarashi
Graduate School of Pharmaceutical Sciences Chiba University
1-8-1 Inohana
Chuo-ku, Chiba 260-8675, Japan

Y. Yamauchi
Department of Pharmaceutical Physical Chemistry
College of Pharmaceutical Sciences, Matsuyama University
4-2, Bunkyo
Matsuyama, Ehime 790-8578, Japan

UV	ultraviolet
VIS light	visible light

INTRODUCTION

Drug-induced phototoxic skin responses are caused after the exposure of skin to photoreactive drugs, triggered by exposure to UVA (320–400 nm) and UVB (290–320 nm) radiation (1,2). There are at least three types of phototoxic skin reactions, including photoirritant, photogenotoxic, and photoallergic cascades, the mechanisms and pathologic features of which are quite different (3). Recently, the level of interest in phototoxicity has markedly increased owing to the awareness among the scientific community of the increased level of UV radiation from the sun reaching the earth. At early phases of the drug discovery process, the development of an efficacious phototoxicity testing system is essential for the avoidance of side effects. Therefore, a number of efforts have been made to provide a model system for the assessment of photosensitive/phototoxic potential through analytical and biochemical methods (1,4–11). Previously, our group proposed three screening systems to predict the phototoxic risk of newly synthesized drug candidates, which include the reactive oxygen species (ROS) assay for predicting phototoxic potential (12–14), the capillary gel electrophoresis-based photocleavage assay (15), and the DNA-binding assay (16) for photogenotoxic risk. In particular, ROS data on photo-irradiated chemicals could be effective for classifying such chemicals as phototoxic and/or photosensitive, since generation of reactive oxygens was found to be responsible for the induction of early photochemical and photobiological events (17).

A high-throughput ROS assay strategy, employing multiwell plates, might be useful as a first screening for phototoxic risk; however, there are some limitations of the ROS assay for screening purposes (18). The current ROS assay system is composed of two independent analytical processes to monitor type I and II photochemical reactions, and they require UV exposure with a high total irradiation energy, resulting in a long run time and data and operational complexity. Improvements to overcome these drawbacks would be of help to increase the productivity and usability of the ROS assay for phototoxicity assessment. Recently, attention has been drawn to the derivatives-of-reactive-oxygen-metabolites (D-ROM) test in the fields of clinical pharmacology and biochemistry (19–21). The D-ROM assay can detect peroxyl or alkoxyl radicals of a generic peroxide, which are indicative of oxidative stress conditions and generation of reactive oxygens (22). Accordingly, the D-ROM assay is currently recognized as an efficient and simplified analytical method for evaluating oxidative stress in the body (20). In addition to its clinical utility, the D-ROM assay might theoretically be applicable to phototoxicity screening by monitoring reactive oxygens-mediated photochemical events, although no efforts have been made to apply the D-ROM assay strategy to phototoxicity prediction.

The present investigation aimed to develop a novel prediction strategy for the phototoxic risk of drug candidates using a simplified D-ROM assay as an alternative to the ROS assay. The assay conditions of the D-ROM assay were optimized, focusing on irradiation time, sensitivity, solvent system, and robustness, and validation of the new assay system was also carried out. The new assay system was applied to 25 model compounds, including 20 phototoxic drugs and 5 non-phototoxic chemicals. To clarify the predictability of the D-ROM-based phototoxicity test, the phototoxic/photogenotoxic potentials of these chemicals were assessed by the ROS assay, the DNA-photocleaving assay, and the *in vitro* 3T3 neutral red uptake phototoxicity test (3T3 NRU PT).

MATERIALS AND METHODS

Chemicals

Naproxen, benzocaine, and sulisobenzone were purchased from Tokyo Chemical Industry (Tokyo, Japan), and 5-fluorouracil (5-FU), 8-methoxypsoralen (8-MOP), amiodarone, diclofenac, dimethyl sulfoxide, doxycycline, furosemide, imipramine, nalidixic acid, piroxicam, promethazine, quinine, and aspirin were purchased from Sigma (St. Louis, MO, USA). Chlorpromazine, *N,N*-diethyl-*p*-phenylenediamine (DEPPD), indomethacin, ketoprofen, nitrofurantoin, norfloxacin, erythromycin, ferrous sulfate, omeprazole, phenytoin, plasmid pBR322 DNA, *p*-nitrosodimethylaniline, imidazole, nitroblue tetrazolium, and quinidine were obtained from Wako Pure Chemical Industries (Osaka, Japan). Agarose L03 was purchased from Takara Bio (Shiga, Japan), and carbamazepine was bought from Acros Organics (Morris Plains, NJ, USA). Ethidium bromide (EtBr) was purchased from Nippon Gene (Toyama, Japan), and acetonitrile was purchased from Kanto Chemical (Tokyo, Japan). A quartz reaction container for high-throughput ROS assay was constructed by Ozawa Science (Aichi, Japan).

D-ROM Assay

The D-ROM assay is a spectrophotometric method that measures the alkoxy and peroxy radicals. D-ROM, generated from photosensitive chemicals under light exposure, were determined in accordance with the procedure of Hayashi *et al.* with some modifications (19). Briefly, assay mixtures containing the tested compounds (200 μM), DEPPD (600 μM), and ferrous sulfate (6.9 μM) in 0.1 M

acetic acid/sodium acetate buffer (pH 4.8) were prepared, and 245 μL of each assay mixture was stored in an Atlas Suntest CPS+solar simulator (Atlas Material Technology LLC, Chicago, USA) equipped with a xenon arc lamp (1,500 W). A UV special filter was installed to adapt the spectrum of the artificial light source to that of natural daylight. The irradiation test was carried out at 25°C with an irradiance of 250 W/m^2 (300–800 nm). Standard assays are typically performed in 96-well microtiter plates, employing a quartz reaction container as we proposed previously (14). After irradiation, the increase in absorbance at 505 nm was measured using a SAFIRE microplate spectrophotometer (TECAN, Männedorf, Switzerland).

ROS Assay

In our previous investigations, ROS assay was designed to detect both singlet oxygen and superoxide generated from photo-irradiated chemicals (13,14). In the ROS assay, each tested compound was stored in a light-irradiation tester Light-Tron Xenon (LTX-01, Nagano Science, Osaka, Japan) equipped with a xenon lamp (2,000 W). The spectral output of the lamps through the optical filter 310 and infrared cutting filter (Nagano Science) was 310–800, with a maximum at 470 nm. The illuminance was set at 30,000 lux, and the irradiation test was carried out at 25°C. Singlet oxygen was measured in an aqueous solution by spectrophotometrically monitoring the bleaching of RNO at 440 nm using imidazole as a selective acceptor of singlet oxygen. Samples containing the compounds under examination, *p*-nitrosodimethylaniline (50 μM) and imidazole (50 μM), in 20 mM sodium phosphate buffer (NaPB) (pH 7.4) were irradiated with UVA/B and Vis light (30,000 lux), and then the UV absorption at 440 nm was measured using a SAFIRE microplate spectrophotometer (TECAN). For the determination of superoxide, samples containing the compounds under examination and nitroblue tetrazolium (NBT, 50 μM) in 20 mM NaPB were irradiated with the UVA/B and Vis light (30,000 lux) for the indicated periods, and the reduction in NBT was measured by the increase in absorbance at 560 nm using a SAFIRE microplate spectrophotometer (TECAN).

DNA Photocleavage

In the DNA photocleavage assay, each assay mixture was stored in an Atlas Suntest CPS+solar simulator (Atlas Material Technology LLC) equipped with a xenon arc lamp (1,500 W) and a UV special filter. The irradiation test was carried out at 25°C with an irradiance of 250 W/m^2 (300–800 nm). The irradiated samples contained pBR322 DNA (final concentration, 10 μg/mL) dissolved in Tris-Acetate-EDTA (TAE) buffer (40 mM Tris, 20 mM boric acid, and 1 mM EDTA; pH 7.4) and the examined compounds at a final concentration of 200 μM. Irradiated plasmid pBR322 DNA was separated by electrophoresis (0.8% agarose gel in TAE buffer), stained with EtBr solution (0.5 μg/mL), and analyzed with image analyzing software Image J.

Atomic Force Microscopy (AFM)

AFM observation of plasmid DNA was carried out using an SPM-9600 scanning probe microscope (Shimadzu Co., Kyoto, Japan) in tapping mode with silicon cantilevers NCHR (NANOWORLD, Neuchâtel, Switzerland) whose spring constant and resonance frequency were 40 N/m and 300 kHz, respectively. The scan frequency was typically 1 Hz per line, and the modulation amplitude was a few nanometers. All samples were imaged in air at room temperature.

In Vitro 3T3 NRU PT

The *in vitro* 3T3 NRU PT was carried out as described in the Organisation for Economic Co-operation and Development (OECD) 432 guideline and the European Community Official Journal (L 136/9, 08.06.2000, annexe II). Briefly, 96-well tissue culture plates were seeded with 1.0×10^4 cells/well 3T3 mouse fibroblast cells. The plates were incubated at 37°C in a humidified 5% CO_2 incubator for 24 h. Cells were exposed to dilutions of the test compounds in Earle's Balanced Salt Solution (EBSS) for 60 min. Compounds were tested at various concentrations ranging from 0.061 to 1,000 μg/mL. Chlorpromazine was used as a positive control. Duplicate plates were exposed for 20 min to UVA light (ca. 50 W/m^2) from UV BIO-SUN illuminator (Vilbert-Lourmat, Marne-la-Vallee, France) or were kept in the dark. After UVA exposure (total energy dose: 5 J/cm^2), the solutions were removed from all plates, and the cells were washed twice with EBSS and DMEM. The cells were then reincubated in culture medium overnight. Cell viability was assessed using the neutral red uptake (NRU) assay (23). The NRU assay consisted of a 3-h incubation with neutral red (50 μg/mL in DMEM) followed by extraction with a mixture (150 μL) of acetic acid, ethanol, and water (1 : 50 : 49). The absorbance was measured at 540 nm. The photo-irritancy factor (PIF) was calculated as an indicator of phototoxicity in accordance with a previous report (24). PIF is calculated by comparing two equally effective cytotoxic concentrations (EC_{50}) of irradiated and non-irradiated chemicals.

Data Analysis

For statistical comparisons, one-way analysis of variance (ANOVA) with pairwise comparison by Fisher's least-

significant-difference procedure was used. A P value of less than 0.05 was considered significant for all analyses. To evaluate the robustness of the D-ROM assay, the Z'-factor, a statistical function, was calculated using the following equation: $Z' = 1 - (3\sigma_{c+} + 3\sigma_{c-})/|\mu_{c+} - \mu_{c-}|$ (25). The means of the positive and negative control signals are denoted as μ_{c+} and μ_{c-}, respectively. The SDs of the signals are denoted as σ_{c+} and σ_{c-}, respectively. The difference between the means, $|\mu_{c+} - \mu_{c-}|$, defines the assay dynamic range.

RESULTS AND DISCUSSION

Generation of D-ROM from UV-Excited Drugs

In phototoxic/photochemical events, the absorption of photon energy could be a key trigger for the photosensitization process, followed by the formation of reactive oxygens, such as superoxide and singlet oxygen through the type I and II reactions, respectively. Currently, these radical species are identified as the principal intermediate species in phototoxic responses (26). In the present investigation, the generation of D-ROM from irradiated drugs was monitored as an indicator for production of reactive oxygens. The generation of D-ROM could be detected using DEPPD, a chromogenic substrate for peroxyl radicals, followed by the formation of colored radical cations of the substrate (19). The exposure of quinine, a typical phototoxic drug, to UVA/B and Vis light (250 W/m^2) led to the marked production of D-ROM in a concentration-dependent manner (Fig. 1a). The generation of D-ROM was thought to be a photodynamic reaction, since quinine, protected from light, did not show potent D-ROM generation. Although it takes as long as 60 min to complete the ROS assay employing the same UV source as we proposed previously (14), the D-ROM assay could be completed within a few minutes, contributing to improved throughput of phototoxicity screening. According to the time evolution of the generation of radicals, taken together with the gradual increase in the basal level and discoloring of the reacted substrate, UV irradiation for 1 min was considered suitable for the D-ROM assay.

Some solvents act as modulators of radical species, so some differences in the generation of reactive oxygens might be observed depending on the solvent system used. For instance, dimethyl sulfoxide and isopropanol were found to act as quenchers of some reactive oxidants (27,28), whereas hexane and deuterium monoxide might stabilize some radical species with an extension of the half-life time (29,30). In our previous study, the use of acetonitrile-containing buffer was proposed for the ROS assay, because of its only slight influence on determination of singlet oxygen and superoxide (14). To clarify the effect of acetonitrile on the new screening system, D-ROM assays on quinine (200 μM) were also carried out in the presence of acetonitrile at various concentrations, ranging from 0 to 50% (Fig. 1b). The influence of acetonitrile at concentrations of less than 30% was negligible as evidenced by the constant outcomes for the D-ROM assay. However, acetonitrile at higher concentrations (>30%) attenuated D-ROM generation from quinine, which was possibly due to an altered photochemical property of quinine or measurement interference. Thus, D-ROM data might depend on the solvent system; therefore, the use of the same solvent system for both stock solution and assay mixture would ensure the most robust D-ROM assay for phototoxic prediction.

Validation of D-ROM Assay for Phototoxic Risk Assessment

To assess the robustness and reproducibility of the D-ROM assay, the Z'-factor was also calculated (25). The Z'-factor is

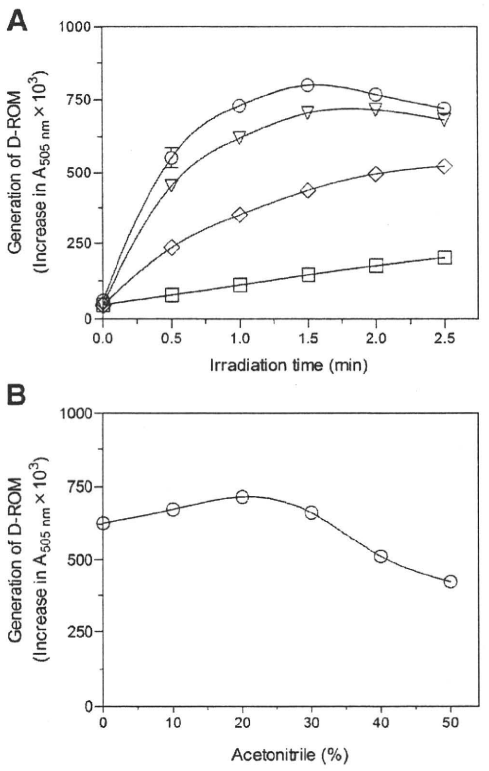

Fig. 1 Generation of D-ROM from photo-irradiated quinine. (A) Time course of D-ROM generation. Quinine was dissolved in 0.1 M acetic acid/sodium acetate buffer (pH4.8) and exposed to simulated sunlight for the indicated periods with an irradiance of 250 W/m^2. □, control (vehicle alone); ◊, quinine at 20 μM; ∇, 100 μM; and ○, 200 μM. Data represent mean ± SD of four determinations. (B) D-ROM generation from irradiated quinine in the presence of acetonitrile. Quinine (200 μM), dissolved in 0.1 M acetic acid/sodium acetate buffer (pH4.8) with various concentrations of acetonitrile, was exposed to simulated sunlight (250 W/m^2) for 1 min. Data represent mean ± SD of four determinations.

designed to reflect both assay signal noise ratio and the variation associated with the signal measurements. Hence, the Z'-factor is commonly utilized for quality assessment in assay development and optimization, as well as evaluation of the reproducibility of assays used for high-throughput screening campaigns (31). In an ideal assay, the Z'-factor is close to 1.0. In practical terms, a Z'-factor greater than 0.5 is indicative of an excellent assay, whereas assays with Z'-factor values less than 0.5 show a small separation band. Typical values from multiple measurements (20 times) of quinine (200 μM) and sulisobenzone (200 μM) are shown in Fig. 2. The Z'-factor for the D-ROM assay was calculated to be 0.75, demonstrating that the assay allows a large separation band between samples and blank signals and thereby confirming its suitability for high-throughput screening.

The overall precision of the method was evaluated by analyzing quinine standard solutions at 20 and 200 μM, and the intra-day precision (%RSD, $n=12$) and inter-day precision (days 1 and 3,%RSD, $n=24$) are shown in Table I. The intra-day%RSD values for the D-ROM assay were calculated to be 6.7 (20 μM) and 3.6 (200 μM), and the inter-day%RSD values were found to be 10.6 (20 μM) and 5.4 (200 μM). Thus, the precision of D-ROM assay at 20 μM was not high enough for high-throughput screening, although the %RSD value at 200 μM was below 6%. These data suggested that the proposed analysis has good intra- and inter-day precisions at higher analyte concentration (200 μM).

Phototoxic Risk Assessment on Model Compounds Using D-ROM Assay

On the basis of the optimized analytical method, the phototoxic risk of model compounds was evaluated (Table II). For comparison, the ROS assay was also carried out on these chemicals, in which both singlet oxygen and superoxide were monitored by independent colorimetrical determination. Of all chemicals tested, 8 phototoxic drugs exhibited significant D-ROM generation when exposed to simulated sunlight, which included chlorpromazine, ketoprofen, nalidixic acid, norfloxacin, omeprazole, promethazine, quinidine, and quinine. Quinidine is a stereoisomer of quinine, and there were no significant differences in photochemical behavior between quinine and quinidine ($p<0.05$), as evidenced by the results from ROS and D-ROM assays. Five non-phototoxic chemicals did not exhibit D-ROM production under light exposure, which was consistent with the results from the ROS assay. In addition to the non-phototoxic chemicals, some phototoxic drugs had no ability to generate D-ROM, whereas high amounts of singlet oxygen and/or superoxide were detected for these chemicals. Interestingly, significant generation of these reactive oxygens was observed for most phototoxic drugs examined, and only 5-FU was found to be less photoreactive among the phototoxic chemicals tested. We expected that D-ROM data could be highly related to the results from the ROS assay. However, there appeared to be a partial discrepancy between ROS and D-ROM data; in particular, the results for 8-MOP, diclofenac, doxycycline, furosemide, naproxen, nitrofurantoin, and piroxicam were quite different. Since the D-ROM assay could be indicative of typical reactive oxygen metabolites, such as alkoxy and peroxy radicals, it has been identified as one of the most reliable indicators of oxidative stress (20). However, the present findings suggested that other chemical pathways are involved in the metabolism of reactive oxygens and that the generated reactive oxygens might be captured via interaction with phototoxins, preventing the reaction with the chromogenic substrate. There also is the probability that non-oxidative photochemical intermediates may be formed under light exposure and that excited drug may

Table I Intra-day and Inter-day (Day 1 and 3) Precision of D-ROM Assay

Quinine concentration (μM)	Generation of D-ROM (Increase in $A_{505\ nm}\times10^3$)
Intra-day	
20	180 ± 12 (6.7)
200	620 ± 22 (3.6)
Inter-day	
20	168 ± 18 (10.6)
200	600 ± 33 (5.4)

Quinine (20 μM and 200 μM) was dissolved in 0.1 M acetic acid/sodium acetate buffer (pH 4.8) and exposed to UVA/B and Vis light (250 W/m^2) for 1 min. Data represent mean ± SD of three repeated experiments for intra-day ($n=12$) precision and six repeated experiments for inter-day precision ($n=24$). Values in parentheses are relative standard deviations.

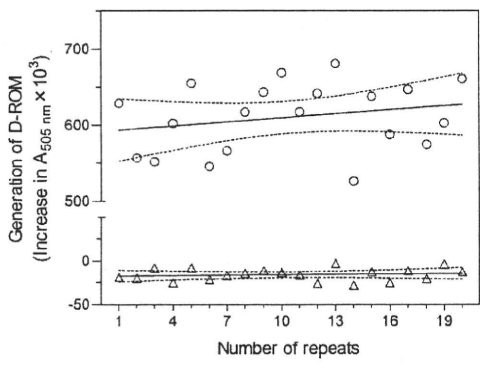

Fig. 2 Representative multiple measurement data used to calculate the Z'-factor for the D-ROM assay. Quinine as positive control (○) or sulisobenzone as negative control (Δ) at a concentration of 200 μM was dissolved in 0.1 M acetic acid/sodium acetate buffer (pH4.8) and exposed to simulated sunlight (250 W/m^2) for 1 min. Lines indicate mean ± 95% confidence interval.

Table II Photochemical and Photobiological Data on 20 Phototoxic and 5 Non-phototoxic Chemicals

Compounds (200μM)	D-ROM ($\Delta A_{505\ nm} \times 10^3$)	ROS data		DNA photocleavage (O.C.:% of total)	3T3 NRU PT (PIF)
		Singlet oxygen ($\Delta A_{440\ nm} \times 10^3$)	Superoxide ($\Delta A_{560\ nm} \times 10^3$)		
Photosensitizers					
5-Fluorouracil	19±1	N.D.	2	5.2	1.0
8-Methoxy psoralen	6±2	272	89	11.0	>74
Amiodarone	23±4	365	N.D.	10.9	7.2
Carbamazepine	<1.0	N.D.	96	4.4	21.9
Chlorpromazine	121±7	59	95	100.0	21.9
Diclofenac	<1.0	181	227	21.7	10.2
Doxycycline	<1.0	510	428	12.4	11.0
Furosemide	<1.0	519	135	10.3	1.0
Imipramine	<1.0	N.D.	100	8.1	1.0
Indomethacin	<1.0	13	121	6.2	1.0
Ketoprofen	151±6	421	97	80.3	110
Nalidixic acid	349±16	428	125	72.4	6.5
Naproxen	<1.0	306	131	34.2	3.7
Nitrofurantoin	<1.0	548	36	4.5	1.0
Norfloxacin	104±13	411	126	23.3	>5.9
Omeprazole	77±11	N.D.	156	52.0	2.7
Piroxicam	<1.0	542	84	5.9	1.0
Promethazine	280±10	286	169	29.1	5.9
Quinidine	630±29	673	115	88.7	29.9
Quinine	632±40	686	124	85.5	15.7
Non-phototoxic chemicals					
Aspirin	7±2	9	2	4.6	1.0
Benzocaine	<1.0	N.D.	25	4.1	1.0
Erythromycin	3±2	N.D.	3	4.7	1.0
Phenytoin	<1.0	N.D.	15	3.5	1.0
Sulisobenzone	<1.0	N.D.	11	5.4	1.0

react with DEPPD directly. Thus, D-ROM assay has some possible limitations, since these photochemical reactions may yield either false positives or negatives.

On the basis of comparison with clinical information on drug-induced phototoxicity (2,32–34), the D-ROM assay might be less predictive of phototoxic risk than the ROS assay. However, the assay procedure for the D-ROM assay was highly simplified with two improvements. First, the D-ROM assay was designed for monitoring only one chromogenic substrate (DEPPD), which might offer reduced system complexity. In contrast, in the ROS assay that we proposed previously, determinations of both singlet oxygen and superoxide were necessary for reliable evaluation (12). Second, there was a marked reduction in screening run time compared with that in the ROS assay. Given these characteristics, especially highly improved throughput, the D-ROM assay might be useful for screening purposes in the drug discovery process.

Relatedness to DNA Photocleavage Assays

For further investigation of the relationship between D-ROM data and photogenotoxic potential, the pBR322 DNA-photocleaving activities of 25 model compounds were evaluated. Generally, DNA strand breaks can be readily observed by the structural conversion of supercoiled pBR322 DNA (SC) to the open circular (OC) form. In the present investigation, the conformation of photosensitized DNA cleavage products was analyzed by AFM (Fig. 3a). In AFM images of the irradiated pBR322 DNA without quinine, most DNA displayed the supercoiled form (Fig. 3a-I). In contrast, the majority of the irradiated DNA with quinine existed in the open circular form, reflecting a single-strand break in the DNA (Fig. 3a-II). The DNA-photocleaving activity of quinine (200 μM) was also analyzed by 0.8% agarose gel electrophoresis with EtBr staining (Fig. 3b). Irradiation of the plasmid DNA alone

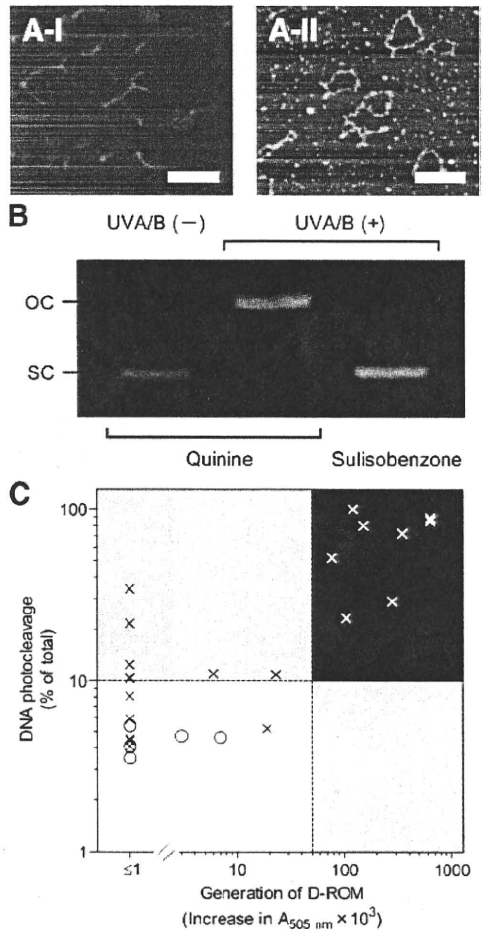

Fig. 3 DNA-photocleavage assay for predicting photogenotoxic potential. **a** AFM images from intact plasmid pBR322 DNA (A-I) and UV-exposed pBR322 DNA with quinine (200 μM; A-II). Scale bars represent 200 nm. **b** Photocleavage of plasmid pBR322 DNA by quinine. Supercoiled DNA was exposed to simulated sunlight (250 W/m^2) for 25 min with or without quinine or sulisobenzone (200 μM). Each pBR322 DNA sample was separated on 0.8% agarose gel and stained with ethidium bromide. OC, open circular form; and SC, supercoiled form. **c** A 2D plot of DNA-photodeavage *versus* D-ROM data for 25 compounds. ×, Phototoxic drugs; and ○, weak/non-phototoxic chemicals. According to tentative classification criteria, plot data were categorized into 3 regions; (1) shaded region, positive in both assays, (2) gray region, positive in only one assay, and (3) white region, negative in both assays.

with UVA/B and Vis light (250 W/m^2) for 25 min did not result in impairment of DNA (data not shown), and the addition of quinine (200 μM) to plasmid DNA also did not result in any structural conversion in the dark. However, significant DNA damage was caused by quinine after UV irradiation, although the DNA-photocleaving activity of sulisobenzone, a non-phototoxic chemical, was negligible under the same experimental condition. On the basis of its band intensity, there appeared to be a ca. 86% structural conversion of plasmid DNA after treatment with irradiated quinine.

The results of the AGE-based DNA photocleavage assay for other chemicals are summarized in Table II. Although non-phototoxic chemicals did not accelerate DNA photocleavage, photosensitizers tended to cause DNA damage upon light exposure. However, not all phototoxic drugs induced photodynamic impairment of DNA. In particular, no significant photocleaving activities were seen for 5-FU, carbamazepine, indomethacin, nitrofurantoin, and piroxicam. For further comparison, the results from DNA-photocleavage and D-ROM assays were analyzed on a 2D plot of DNA impairment *versus* D-ROM generation for various pharmaceutical substances (Fig. 3c). The plot data were categorized into 3 regions with tentative classification criteria: 10% DNA damage in DNA-photocleavage assay and 5×10^{-2} AU for D-ROM assay. Compounds in the shaded region were predicted as high risk in both assays. Chemicals in gray regions were predicted to have phototoxic risk by only one assay. Phototoxic/photogenotoxic risk was considered negligible for chemicals lying in the white region. Of all tested compounds, only 6 chemicals (24% of the total), including 8-MOP, amiodarone, diclofenac, doxycycline, furosemide and naproxen, can be found in the gray regions. From these findings, the D-ROM assay was shown to predict drug-induced DNA damage, reflecting photogenotoxic potential, with a prediction accuracy of 76%.

UV absorption usually generates singlet excited states. Although they are too short-lived to react chemically, more stable excited triplet states are sometimes formed by intersystem crossing, leading to direct and/or indirect DNA damage (2). In the photogenotoxic pathways, there are at least three direct mechanisms (35). First, photo-excited species sometimes induce direct DNA damage by covalent binding, resulting in formation of photoadducts. Second, an excited molecule can transfer the excitation energy to DNA, leading to pyrimidine dimer formation as observed upon direct DNA excitation. Last, photo-excited chromophore induces a one-electron or hydrogen abstraction, and the resulting DNA damage appears to consist mostly of oxidative guanine modification. In addition to these direct mechanisms of DNA damage by excited photoreactive chemicals, there are also at least two indirect mechanisms, which include (1) reactive oxygens-mediated DNA impairment and (2) generation of reactive decomposition products. Thus, possible mechanisms for photochemical genotoxicity can be quite complex and may involve a series of chemical reactions. All phototoxins might not always cause reactive oxygens-mediated photogenotoxic reactions, so that some phototoxins could not be captured by D-ROM assay. This might partially explain the data discrepancy between DNA-photocleavage and D-ROM assays.

Relatedness to 3T3 Neutral Red Uptake Phototoxicity Test

The 3T3 NRU PT was developed and validated under the auspices of ECVAM from 1992–1997 to establish a valid *in vitro* alternative to the various *in vivo* tests in use (36). The test is now accepted by the European Union commission and member states as being necessary for all compounds showing absorbance of UVA and Vis light (37). The 3T3 NRU PT assesses the cytotoxic effect of a test substance after exposure to a non-cytotoxic dose of UVA light compared with that in the absence of exposure, and the cytotoxicity is expressed as a concentration-dependent reduction in the uptake of Neutral Red. In this investigation, the viability curves of model compounds with or without irradiation were determined up to 1 mg/mL. Fig. 4a shows representative cell viability curves of the 3T3 cells after exposure to quinine and sulisobenzone. With respect to the quinine-treated group, upon irradiation, the cell viability was shifted to considerably lower concentrations. The EC_{50} values with and without UVA irradiation were 9.7 μg/mL and 150 μg/mL, respectively. These values produced a PIF of 15.7 for quinine. In contrast, the cell viability curve for 3T3 cells after exposure to irradiated sulisobenzone was almost identical to that without UVA exposure. Thus, the PIF value of sulisobenzone was calculated to be 1.0. Generally, PIF values are effective for distinguishing phototoxic molecules (PIF>5) from non-phototoxic molecules, but are actually unable to correctly distinguish between mildly or probably phototoxic molecules (2<PIF<5) and non-phototoxic molecules (PIF<2). On the basis of the classification criteria of PIF value, quinine was found to be phototoxic. In addition to quinine and sulisobenzone, the phototoxic potentials of other chemicals were also assessed by 3T3 NRU PT for further comparison (Table II). Of all phototoxic drugs, 14 phototoxic drugs (70% of all phototoxins) exhibited a potent phototoxic effect on cells as evidenced by a high PIF value (>2). However, some known phototoxic drugs, such as 5-FU, furosemide, imipramine, indomethacin, nitrofurantoin, and piroxicam, showed no significant transition in viability curves with or without UVA irradiation. Their PIF values (ca. 1.0) suggested a low phototoxic potential, and these findings were inconsistent with the results from DNA-photocleavage and D-ROM assays. On the basis of the present 3T3 NRU PT data and the adverse event information on the model chemicals listed in drug package inserts and several manuscripts (1,2,34,38), the prediction accuracy of 3T3 NRU PT was calculated to be 76%. The limited predictability of 3T3 NRU PT is not surprising since bioavailability and biokinetics can not be modeled in the assay, and it may result in the lack of *in vivo-in vitro* correlation (4).

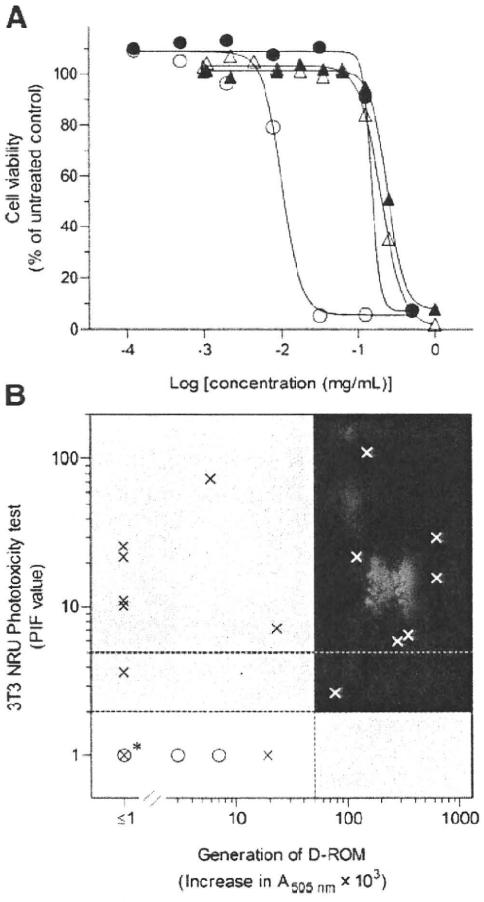

Fig. 4 *In vitro* phototoxicity assessment. **a** Phototoxicity of tested compounds in the 3T3 NRU PT. The 3T3 cells were treated with different concentrations of quinine or sulisobenzone, and irradiated with UVA light (50 kJ/m^2). Each value represents the mean of 6 replicates. ●, quinine without UVA (control); ○, quinine with UVA; ▲, sulisobenzone without UVA (control); and Δ, sulisobenzone with UVA. **b** A 2D plot of 3T3 NRU PT data *versus* D-ROM data for 25 compounds. ×, Phototoxic drugs; and ○, weak/non-phototoxic chemicals. According to tentative classification criteria, plot data were categorized into 3 regions; (1) shaded region, positive in both assays, (2) gray region, positive in only one assay, and (3) white region, negative in both assays. *, Overlapped symbols of 5 phototoxic and 3 non-phototoxic chemicals.

According to the 2D plot analysis of D-ROM and 3T3 NRU PT data (Fig. 4b), tested chemicals were categorized into three regions: 11 chemicals in the white region (both negative), 7 chemicals in the gray region (only one positive), and 7 chemicals in the shaded region (both positive). There is an empirical correlation of 72% between these two assays, and the exact reasons for the discrepancy are not fully understood. The 3T3 NRU PT can only use irradiation in the UVA, since UVB light is highly cytotoxic to the Balb/c 3T3 cells. Although UVB wavelengths are excluded in the 3T3 NRU PT, these wavelengths are an integral part of solar radiation responsible for photochemical reactions. Herein, the difference in irradiation condition might be a

part of the reason for data discrepancy between the 3T3 NRU PT and D-ROM assay. In addition, some phototoxins can induce phototoxic skin responses via reactive oxygens-independent pathways, and they may bind with lipids and proteins, as well as DNA (2). Photo-induced reactions with these biomolecules are important to the development of phototoxic and/or photoallergic responses (1). D-ROM assay can not completely predict the phototoxic risk as long as the photochemical reaction is reactive oxygens-independent. Further clarification will be helpful for understanding the limitations of the D-ROM assay and avoiding misleading data.

Previously, Lynch and co-workers demonstrated the link between phototoxicity and photoreactivity, and they proposed 3 key photochemical reactivity parameters, including the production of singlet oxygen, the production of superoxide, and the chemical photostability (11). Based on these findings, the photochemical reactivity assays may provide a good predictor of phototoxic liability *in vitro*. The extension of the photostability testing to assess potential phototoxic responses has already been included in the risk assessment strategy by the CPMP guidance on photosafety testing. In contrast, Henry and co-workers demonstrated that photostability testing alone was an inadequate predictor of possible photosafety liabilities, although the measurement of light absorption seemed to be a contributing part of an overall pre-clinical photosafety risk assessment process (4). Although the most reliable photoreactivity parameters are still under discussion, combination use of the efficacious photoreactive parameters may be useful for prediction of potential photosafety issues. Attempts to increase the predictability of D-ROM assay may need a further knowledge of the complex photochemical reaction pathways, and the combination use of D-ROM assay and other reliable predicting tools may provide a more reliable risk assessment strategy for the screening of the phototoxic potential of new drug entities in early development.

CONCLUSION

In the present investigation, an optimized D-ROM assay system was proposed for predicting the phototoxic potential of pharmaceutical substances. The photochemical and phototoxic behaviors of 25 model compounds were assessed by the ROS assay, the DNA-photocleavage test, and the 3T3 NRU PT, as well as the D-ROM assay, for comparison. The results from the D-ROM assay did not completely correlate with the ROS data; however, the D-ROM assay was partly indicative of photogenotoxic risk, as identified by the DNA photocleavage test, and phototoxic potential, as proposed by the 3T3 NRU PT, with prediction accuracies of 76 and 72%, respectively. These outcomes, taken together with the high-throughput contributing to highly reduced screening run time, suggest the usefulness of the D-ROM assay for identifying phototoxic potential and avoiding undesired side effects in the early stages of drug discovery.

ACKNOWLEDGEMENTS

This work was supported in part by a Grant-in-Aid from the Food Safety Commission, Japan (No. 0807).

REFERENCES

1. Onoue S, Seto Y, Gandy G, Yamada S. Drug-induced phototoxicity; an early *in vitro* identification of phototoxic potential of new drug entities in drug discovery and development. Curr Drug Saf. 2009;4:123–36.
2. Moore DE. Drug-induced cutaneous photosensitivity: incidence, mechanism, prevention and management. Drug Saf. 2002;25:345–72.
3. Epstein JH, Wintroub BU. Photosensitivity due to drugs. Drugs. 1985;30:42–57.
4. Henry B, Foti C, Alsante K. Can light absorption and photostability data be used to assess the photosafety risks in patients for a new drug molecule? J Photochem Photobiol B. 2009;96:57–62.
5. Epstein S. The Photopatch Test; Its Technique, Manifestations, And Significance. Ann Allergy. 1964;22:1–11.
6. Przybilla B, Schwab-Przybilla U, Ruzicka T, Ring J. Phototoxicity of non-steroidal anti-inflammatory drugs demonstrated *in vitro* by a photo-basophil-histamine-release test. Photodermatol. 1987;4:73–8.
7. Selvaag E. Evaluation of phototoxic properties of oral antidiabetics and diuretics. Photohemolysis model as a screening method for recognizing potential photosensitizing drugs. Arzneimittelforschung. 1997;47:1031–4.
8. Portes P, Pygmalion MJ, Popovic E, Cottin M, Mariani M. Use of human reconstituted epidermis Episkin for assessment of weak phototoxic potential of chemical compounds. Photodermatol Photoimmunol Photomed. 2002;18:96–102.
9. Spielmann H, Liebsch M, Doring B, Moldenhauer F. First results of an EC/COLIPA validation project of *in vitro* phototoxicity testing methods. Altex. 1994;11:22–31.
10. Sarabia Z, Hernandez D, Castell JV, van Henegouwen GM. Photoreactivity of tiaprofenic acid and suprofen using pig skin as an *ex vivo* model. J Photochem Photobiol B. 2000;58:32–6.
11. Lynch AM, Smith MD, Lane AS, Robinson SA, Kleinman MH, Kennedy-Gabb S, Wilcox P, Rees RW. An evaluation of chemical photoreactivity and the relationship to photogenotoxicity. Regul Toxicol Pharmacol. 2009; in press.
12. Onoue S, Tsuda Y. Analytical studies on the prediction of photosensitive/phototoxic potential of pharmaceutical substances. Pharm Res. 2006;23:156–64.
13. Onoue S, Yamauchi Y, Kojima T, Igarashi N, Tsuda Y. Analytical studies on photochemical behavior of phototoxic substances; effect of detergent additives on singlet oxygen generation. Pharm Res. 2008;25:861–8.
14. Onoue S, Igarashi N, Yamada S, Tsuda Y. High-throughput reactive oxygen species (ROS) assay: an enabling technology for screening the phototoxic potential of pharmaceutical substances. J Pharm Biomed Anal. 2008;46:187–93.
15. Onoue S, Igarashi N, Kitagawa F, Otsuka K, Tsuda Y. Capillary electrophoretic studies on the photogenotoxic potential of pharmaceutical substances. J Chromatogr A. 2008;1188:50–6.

16. Onoue S, Seto Y, Oishi A, Yamada S. Novel methodology for predicting photogenotoxic risk of pharmaceutical substances based on reactive oxygen species (ROS) and DNA-binding assay. J Pharm Sci. 2009;98:3647–58.
17. Gocke E, Albertini S, Chetelat AA, Kirchner S, Muster W. The photomutagenicity of fluoroquinolones and other drugs. Toxicol Lett. 1998;102–103:375–81.
18. Onoue S, Kawamura K, Igarashi N, Zhou Y, Fujikawa M, Yamada H *et al.* Reactive oxygen species assay-based risk assessment of drug-induced phototoxicity: classification criteria and application to drug candidates. J Pharm Biomed Anal. 2008;47:967–72.
19. Hayashi I, Morishita Y, Imai K, Nakamura M, Nakachi K, Hayashi T. High-throughput spectrophotometric assay of reactive oxygen species in serum. Mutat Res. 2007;631:55–61.
20. Salardi S, Zucchini S, Elleri D, Grossi G, Bargossi AM, Gualandi S *et al.* High glucose levels induce an increase in membrane antioxidants, in terms of vitamin E and coenzyme Q10, in children and adolescents with type 1 diabetes. Diab Care. 2004;27:630–1.
21. Cornelli U, Terranova R, Luca S, Cornelli M, Alberti A. Bioavailability and antioxidant activity of some food supplements in men and women using the D-Roms test as a marker of oxidative stress. J Nutr. 2001;131:3208–11.
22. Alberti A, Bolognini L, Macciantelli D, Caratelli M. The radical cation of N,N-diethyl-para-phenylendiamine: a possibe indicator of oxidative stress in biological samples. Res Chem Intermed. 2000;26:253–67.
23. Borenfreund E, Puerner JA. Toxicity determined *in vitro* by morphological alterations and neutral red absorption. Toxicol Lett. 1985;24:119–24.
24. Peters B, Holzhutter HG. *In vitro* phototoxicity testing: development and validation of a new concentration response analysis software and biostatistical analyses related to the use of various prediction models. Altern Lab Anim. 2002;30:415–32.
25. Zhang JH, Chung TD, Oldenburg KR. A Simple Statistical Parameter for Use in Evaluation and Validation of High Throughput Screening Assays. J Biomol Screen. 1999;4:67–73.
26. Foote CS. Definition of type I and type II photosensitized oxidation. Photochem Photobiol. 1991;54:659.
27. Hei TK, Liu SX, Waldren C. Mutagenicity of arsenic in mammalian cells: role of reactive oxygen species. Proc Natl Acad Sci USA. 1998;95:8103–7.
28. Schwarzenbach RP, Gschwend PM, Imboden DM. Environmental organic chemistry. New York: Wiley; 1993.
29. Keum YS, Kim JH, Kim YW, Kim K, Li QX. Photodegradation of diafenthiuron in water. Pest Manag Sci. 2002;58:496–502.
30. Epe B. Genotoxicity of singlet oxygen. Chem Biol Interact. 1991;80:239–60.
31. Rega MF, Reed JC, Pellecchia M. Robust lanthanide-based assays for the detection of anti-apoptotic Bcl-2-family protein antagonists. Bioorg Chem. 2007;35:113–20.
32. Dubakiene R, Kupriene M. Scientific problems of photosensitivity. Medicina (Kaunas). 2006;42:619–24.
33. Gould JW, Mercurio MG, Elmets CA. Cutaneous photosensitivity diseases induced by exogenous agents. J Am Acad Dermatol. 1995;33:551–73. quiz 574–6.
34. Allen JE. Drug-induced photosensitivity. Clin Pharm. 1993;12:580–7.
35. Brendler-Schwaab S, Czich A, Epe B, Gocke E, Kaina B, Muller L *et al.* Photochemical genotoxicity: principles and test methods. Report of a GUM task force. Mutat Res. 2004;566:65–91.
36. Liebsch M, Spielmann H. Currently available *in vitro* methods used in the regulatory toxicology. Toxicol Lett. 2002;127:127–34.
37. EMEA Report. Committee for propriety medicinal products (CPMP). Notes for guidance on photosafety testing CPMP/SWP/398/01. http://www.emea.europa.eu/pdfs/human/swp/039801en.pdf; 2002.
38. Stein KR, Scheinfeld NS. Drug-induced photoallergic and phototoxic reactions. Expert Opin Drug Saf. 2007;6:431–43.

Journal of Pharmaceutical and Biomedical Analysis 52 (2010) 781–786

Contents lists available at ScienceDirect

Journal of Pharmaceutical and Biomedical Analysis

journal homepage: www.elsevier.com/locate/jpba

Short communication

High-throughput screening strategy for photogenotoxic potential of pharmaceutical substances using fluorescent intercalating dye

Yoshiki Seto, Masanori Ochi, Satomi Onoue *, Shizuo Yamada

Department of Pharmacokinetics and Pharmacodynamics and Global Center of Excellence (COE) Program, School of Pharmaceutical Sciences, University of Shizuoka, 52-1 Yada, Suruga-ku, Shizuoka 422-8526, Japan

ARTICLE INFO

Article history:
Received 28 December 2009
Received in revised form 17 February 2010
Accepted 19 February 2010
Available online 25 February 2010

Keywords:
Photogenotoxicity
Reactive oxygen species
Thiazole orange
Plasmid DNA
Assay validation

ABSTRACT

The aim of the present study was to provide an intercalator-based photogenotoxicity (IBP) assay as a high-throughput *in vitro* screening system for predicting the photogenotoxic potential of pharmaceutical substances. The conditions of the high-throughput IBP assay using thiazole orange (TO), a fluorescent intercalating dye, were optimized and validated by a fluorescence titration experiment and reproducibility/robustness test. The IBP assay was applied to 27 phototoxic and 5 weak/non-phototoxic commercially available compounds, and other phototoxicity screenings were also carried out for comparison; these included the reactive oxygen species (ROS) assay for overall phototoxic potential and the DNA-photocleavage assay for photogenotoxic risk. According to the results from the comparative experiments, a decreased level of intercalated TO in the IBP assay could theoretically be related to the DNA-photocleaving behaviors of phototoxic drugs, but not to their ROS-generating abilities. The IBP assay could predict the photodynamic DNA impairment caused by irradiated drugs with a prediction accuracy of 78%. These findings suggest that the IBP assay could be a fast and reliable tool for predicting the photogenotoxic potential of a large number of drug candidates at early stages of drug discovery.

1. Introduction

Drug-induced phototoxic skin responses are elicited after the exposure of skin to topical or systemic administration of pharmaceutical substances, triggered by exposure to sunlight [1]. There are at least three types of drug-induced phototoxic reactions, including photoirritation, photoallergy, and photogenotoxicity, the mechanisms and pathologic features of which are quite different [2]. To avoid side effects at an early phase of the drug discovery process, our group previously proposed a reactive oxygen species (ROS) assay for evaluating the phototoxic potential of pharmaceutical substances [3]. However, the ROS assay might lack specificity for three types of phototoxic reactions, since phototoxic compounds do not always exhibit all phototoxic reactions [4–6]. Therefore, other efficacious screening strategies should be developed to predict each type of phototoxic response in more detail.

Over the past few years, the development of effective methodologies to evaluate photogenotoxicity has been attempted, and a number of screening methods for recognizing photogenotoxic drugs have been suggested [7,8]. Our group also proposed novel *in vitro* tools for assessing photogenotoxic risk using capillary gel electrophoresis (CGE) analysis [9] and DNA-binding assay as a second screening tool following ROS assay [10]. Although these assays proposed possible mechanisms of drug-induced photogenotoxicity, some technical problems were encountered, most notably limited throughput in early stages of drug discovery. Improvement of the photogenotoxicity assay is necessary in terms of enhancing reliability and productivity, which could possibly lead to the development of a novel high-throughput screening system. Previously, ethidium bromide (EtBr), an intercalating dye, was used as a fluorescent probe to demonstrate the metal-catalyzed impairment of DNA in the base-pair region [11]. Theoretically, the photogenotoxic potential of photosensitizers is also predictable by intercalator-based screening, since oxidative DNA damage is observed upstream of drug-induced photogenotoxicity [2]. An intercalator-based screening system for oxidative DNA damage using multiwell plates might be efficacious for screening a number of new drugs with high reproducibility, although the assay has never been applied to photogenotoxicity prediction.

The present study aimed to provide an intercalator-based photogenotoxicity (IBP) assay as a more effective and streamlined *in vitro* assessment tool for predicting drug-induced photogenotoxicity. For evaluating the drug-induced impairment of DNA, thiazole orange (TO), a highly sensitive intercalating dye, was used as a fluorescent probe in the IBP assay. TO itself is virtually non-fluorescent, however, the intercalation of DNA with TO was found to result in a 3000-fold enhancement of fluorescence [12,13]. The assay systems were optimized and validated using ketoprofen as a model com-

* Corresponding author. Tel.: +81 54 264 5633; fax: +81 54 264 5635.
E-mail address: onoue@u-shizuoka-ken.ac.jp (S. Onoue).

0731-7085/$ – see front matter © 2010 Elsevier B.V. All rights reserved.
doi:10.1016/j.jpba.2010.02.029

pound with focus on irradiation conditions and concentration of assay mixture. The IBP assay system was applied to 27 photosensitizers and 5 non-phototoxic compounds, and the data obtained were also compared with the results from a ROS assay and an agarose gel electrophoresis (AGE)-based DNA-photocleavage assay to clarify the predictability of the IBP assay.

2. Materials and methods

2.1. Chemicals

All phototoxic and weak/non-phototoxic compounds were purchased from Sigma (St. Louis, MO, USA), Wako Pure Chemical Industries (Osaka, Japan), or Tokyo Chemical Industry (Tokyo, Japan). Salmon sperm DNA, plasmid pBR322 DNA, *p*-nitrosodimethylaniline (RNO), imidazole, nitroblue tetrazolium (NBT), disodium hydrogenphosphate, sodium dihydrogenphosphate dihydrate, and thiazole orange (TO) were bought from Wako Pure Chemical Industries. Ethidium bromide (EtBr) and agarose L03 were purchased from Nippon Gene (Toyama, Japan) and Takara Bio (Shiga, Japan), respectively.

2.2. Fluorescence titration

A fluorescence titration experiment was carried out to optimize the TO concentration for the IBP assay. In a 96-well microplate (AGC Techno Glass, Chiba, Japan), 10 μL of DNA solution (100 μg/mL), dissolved in 20 mM sodium phosphate buffer (NaPB, pH 7.4), was mixed with 20 μL of 20 mM NaPB (pH 7.4) and 70 μL of TO at various final concentrations, ranging from 0.01 to 3 μM. The assay mixtures were incubated at 37 °C for 15 min. After equilibration, the fluorescence (excitation, 509 nm; and emission, 527 nm) of each mixture (100 μL) in the 96-well microplate was measured with SAFIRE (TECAN, Männedorf, Switzerland).

2.3. Irradiation conditions

Each tested compound was stored in an Atlas Suntest CPS+ solar simulator (Atlas Material Technology LLC, Chicago, USA) equipped with a xenon arc lamp (1500 W). A UV special filter and a window glass filter were installed to adapt the spectrum of the artificial light source to natural daylight. The irradiation test was carried out at 25 C with an irradiance of 250 W/m^2.

2.4. Intercalator-based photogenotoxicity (IBP) assay

The photodynamic impairment of salmon sperm DNA by phototoxic chemicals was evaluated by IBP assay. Each assay mixture (50 μL) in the 96-well microplate, containing the tested compound (200 μM) and DNA (20 μg/mL) in 20 mM NaPB (pH 7.4), was irradiated with UVA/B for 45 min, and then TO was added to each well at a final concentration of 1.3 μM. As a control experiment, only 40 μL of the tested compound in 20 mM NaPB (pH 7.4) was exposed to UVA/B, and then DNA (10 μg/mL) and TO (1.3 μM) were added to the sample. In both irradiation and control experiments, each assay mixture (100 μL) was incubated at 37 °C for 15 min to equilibrate intercalation of DNA with TO. To detect the intercalated TO, fluorescence (excitation: 509 nm and emission: 527 nm) was measured with SAFIRE.

2.5. Determination of reactive oxygen species (ROS)

Both singlet oxygen and superoxide generated from irradiated chemicals were measured as we reported previously [14,15]. Briefly, to monitor the generation of singlet oxygen samples containing the compounds under examination, *p*-nitrosodimethylaniline (50 μM) and imidazole (50 μM) in 20 mM NaPB (pH 7.4), were irradiated with UVA/B, and then the UV absorption at 440 nm was measured by SAFIRE. For the determination of superoxide, samples containing the compounds under examination and nitroblue tetrazolium (NBT, 50 μM) in 20 mM NaPB (pH 7.4) were irradiated with UVA/B, and the reduction of NBT was measured by the increase in the absorbance at 560 nm using SAFIRE.

2.6. DNA-photocleavage assay

The irradiated samples contained pBR322 DNA (final concentration, 10 μg/mL) dissolved in Tris–acetic acid–EDTA (TAE) buffer (40 mM Tris, 20 mM acetic acid, and 1 mM EDTA) and the tested compounds at a final concentration of 200 μM. Samples were exposed to UVA/B (375 kJ/m^2). Irradiated plasmid pBR322 DNA was separated by electrophoresis (0.8% agarose gel in TAE buffer), visualized with EtBr staining, and analyzed with image analyzing software Image J.

2.7. Data analysis

For statistical comparisons, a one-way analysis of variance (ANOVA) with pairwise comparison by Fisher's least significant difference procedure was used. A *P*-value of less than 0.05 was considered significant for all analyses.

3. Results and discussion

3.1. Development of IBP assay

Some fluorescent intercalating dyes, such as EtBr and TO, form an intense fluorescent complex with DNA [11,13]. Interestingly, the fluorescent yield is reduced upon DNA denaturation by oxidative stress and becomes very weak when intramolecular hydrogen bonds in single strands are further destabilized [16]. Thus, the intercalating behavior of DNA-specific fluorescent probes should reflect oxidative-stress-induced alterations in the DNA base-pair region. In the present study, to evaluate DNA damage due to photoirradiated compounds, an IBP assay was developed with the use of fluorescent intercalating dyes. TO was chosen for the IBP assay because of a 150-fold higher sensitivity than EtBr. Upon a fluorescence titration experiment, the binding constant of TO with DNA was calculated to be as low as 360 nM. To evaluate DNA impairment with a high sensitivity, the concentration of TO in the IBP assay was set at 1.3 μM, equivalent to the concentration at 80% of maximum binding (data not shown). In addition to the TO concentration, other conditions for the IBP assay, such as UVA/B irradiation time and concentration of compounds, were also optimized using ketoprofen, a typical phototoxic drug. After concomitant exposure of ketoprofen and DNA to UVA/B for the indicated periods, TO was added to the assay mixture to monitor the intercalating behavior (Fig. 1A). Although no significant changes in the intercalating behavior of TO were observed as long as samples were protected from light, the UVA/B exposure of ketoprofen and DNA resulted in a marked reduction in TO-intercalating capacity. The reduction in intercalated TO is indicative of oxidative impairment of DNA, and the photodynamic DNA damage appeared to be saturated at 45 min. According to the concentration response curve (Fig. 1B), only a slight reduction in intercalated TO was observed at 300 μM ketoprofen without UV exposure, whereas irradiated ketoprofen at just over 30 μM caused significant DNA damage.

3.2. Assay precision and robustness

The overall precision of the method was evaluated by analyzing the photogenotoxic potential of ketoprofen standard solution

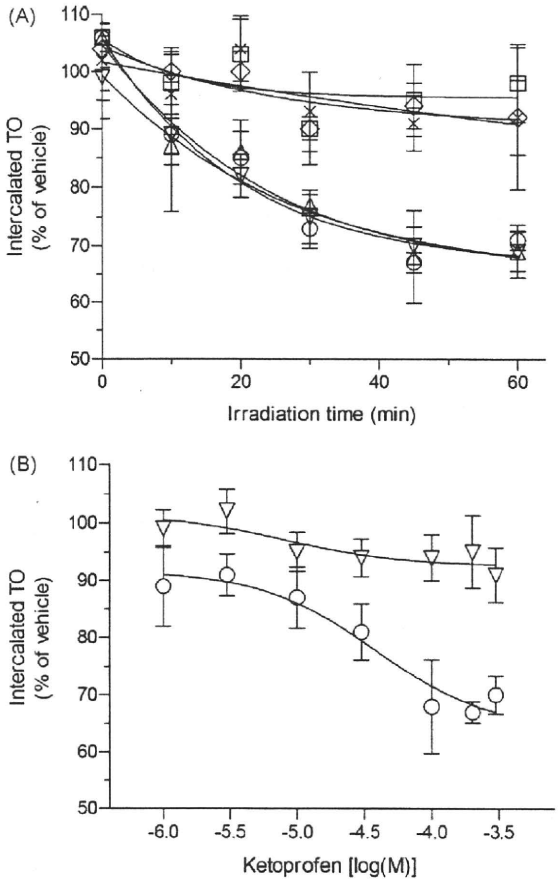

Fig. 1. DNA damage induced by ketoprofen. (A) Time-dependent damage of salmon sperm DNA. Irradiated group: △, 100 μM; ○, 200 μM; and ▽, 300 μM; and control group: ◇, 100 μM; □, 200 μM; and ×, 300 μM. (B) Ketoprofen-induced DNA damage occurred in a dose-dependent manner. Ketoprofen was irradiated with UVA/B in the presence or absence of salmon sperm DNA. ○, Irradiated data; ▽, control data. Data represent mean ± SD of four experiments.

at 100, 200, and 300 μM under 45-min UV exposure. The intra-day precision (%RSD, $n = 3$) and inter-day precision (days 1 and 2%RSD, $n = 6$) are shown in Table 1. The intra-day %RSD values for irradiated and control experiments ranged from 2.98 to 6.86 and 5.12 to 5.51, respectively, and the inter-day %RSD values varied from 5.91 to 6.65 (irradiated group) and 4.97 to 5.27 (control group). On the basis of the data for ketoprofen at 100–300 μM, the IBP assay had potent intra- and inter-day precision, and the concentration of

Table 1
Intra-day and inter-day precision for DNA damage by irradiated ketoprofen.

Concentration (μM)	Intercalated TO [% of vehicle, mean ± SD (%RSD)]	
	Irradiated	Control
Intra-day		
100	72.9 ± 5.00 (6.86)	96.0 ± 4.92 (5.12)
200	76.4 ± 2.27 (2.98)	93.5 ± 4.87 (5.21)
300	76.2 ± 3.93 (5.16)	92.2 ± 5.08 (5.51)
Inter-day		
100	71.6 ± 4.67 (6.53)	95.4 ± 4.74 (4.97)
200	74.0 ± 4.37 (5.91)	93.9 ± 4.91 (5.22)
300	75.3 ± 5.01 (6.65)	93.5 ± 4.93 (5.27)

Ketoprofen (200 μM) and salmon sperm DNA (20 μg/mL) were co-exposed to UVA/B light (675 kJ/m^2) or protected from light. TO (1.3 μM) solution was added to the assay mixture, and fluorescence emitted from the intercalated TO was measured. Data represent mean ± SD of three experiments for intra-day precision and six experiments for inter-day precision.

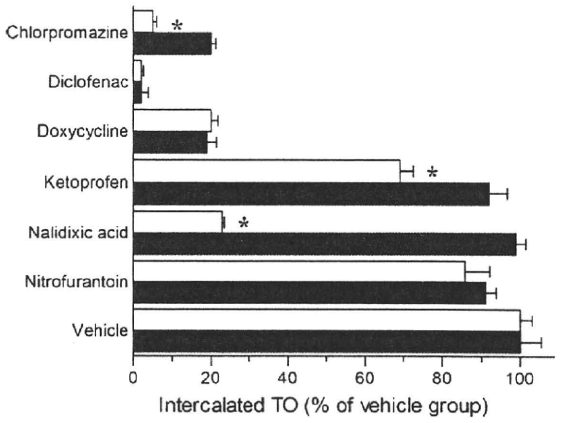

Fig. 2. DNA damage by irradiated phototoxic drugs. Each drug (200 μM) and salmon sperm DNA (20 μg/mL) were co-exposed to UV or protected from light. TO solution at a final concentration of 1.3 μM was added to the assay mixture, and fluorescence emitted from the intercalated TO was measured. Open bar, UV-irradiated; and filled bar, control group. Data represent mean ± SD of four experiments. *$P < 0.05$, significantly different from control.

tested chemicals for the IBP assay was set at 200 μM. Further evaluation on robustness of the IBP assay was also made with emphasis on the influences of co-existing solvents in the assay mixtures and equilibration temperature. By the use of stock solution of tested chemicals, small quantity of organic solvent could be involved in the assay mixture, and this might lead to variable outcomes. However, there were no significant differences among the results from IBP assay of ketoprofen (200 μM) with or without organic solvents (1%) such as dimethyl sulfoxide (DMSO), acetonitrile, methanol, and ethanol (data not shown). In addition, transition of equilibration temperature (25–40 °C) did not affect the IBP data (data not shown).

3.3. Application of IBP assay to known phototoxic/non-phototoxic drugs

The IBP assay was carried out on 27 phototoxic and 5 weak/non-phototoxic commercially available drugs to clarify the predictability and usefulness of the IBP assay. According to the results from the IBP assay on several phototoxic drugs (Fig. 2), ketoprofen, nalidixic acid, and nitrofurantoin did not affect the intercalating behavior of TO without UV exposure. The UV irradiation of ketoprofen and nalidixic acid in the presence of DNA resulted in 23 and 76% reductions in the level of intercalated TO, respectively, although nitrofurantoin was found to be less photogenotoxic as evidenced by the lack of a significant difference in the intercalation of TO between control and irradiated groups. These data were consistent with previous observations on CGE analyses, which showed that both ketoprofen and nalidixic acid could cause photocleavage of plasmid pBR322 DNA, but nitrofurantoin did not [9]. The IBP assay could be applied to most test compounds; however, some drugs, including chlorpromazine, diclofenac, and doxycycline, affected the intercalating behavior of TO without light exposure, leading to a narrow screening window. The decrease in intercalated TO levels might be attributable to drug-induced quenching of fluorescence from DNA-TO complexes and/or strong intercalation between DNA and the drugs. On the basis of the decrease in intercalated TO levels, chlorpromazine might have photogenotoxic potential; however, doxycycline did not seem to be photogenotoxic. It would be very challenging to evaluate the photogenotoxic risk of diclofenac precisely, because of the very limited screening range. Thus, the IBP assay might not be suitable for some chemicals that lack an adequate assay range.

Table 2
Photochemical and photogenotoxic data on phototoxic compounds.

Compounds	ROS generation[a]		DNA photocleavage (OC form, %)	Decrease in intercalated TO (% of vehicle)
	$^1O_2$ ($\Delta A_{440} \times 10^3$)	O_2^- ($\Delta A_{560} \times 10^3$)		
Phototoxic				
5-FU	5±3	N.D.	5.2	N.D.
8-MOP	31±7	51±3	11.0	1
Acetazolamide	19±1	N.D.	2.4	4
Amitriptyline	4±2	8±10	9.9	1
Carbamazepin	7±1	N.D.	4.4	6
Chlorpromazine	N.D.	113±1	100	15*
Clomipramine	60±4	11±1	91.5	24*
Diazepam	12±4	N.D.	4.3	2
Diclofenac	181±7	370±14	21.7	N.D.
Doxycycline	131±8	344±6	12.4	N.D.
Flutamide	25±9	N.D.	10.6	11*
Furosemide	139±5	111±16	10.3	4
Imipramine	21±1	16±1	8.1	15*
Indomethacin	8±4	186±16	N.D.	N.D.
Ketoprofen	348±12	45±5	73.9	23*
Methotrexate	206±17	425±27	8.2	53*
Nalidixic acid	132±2	231±2	72.4	76*
Naproxen	172±7	207±2	34.2	53*
Nitrazepam	174±9	49±5	34.2	61*
Nitrofurantoin	72±7	15±1	4.5	5
Omeprazole	25±7	150±1	52.0	15*
Oxytetracycline	257±21	275±18	6.5	N.D.
Piroxicam	83±7	96±9	5.9	5
Promethazine	52±4	34±2	29.1	18*
Quinine	376±11	240±6	85.5	38*
Tetracycline	203±29	169±13	10.4	6
Tolbutamide	1±6	N.D.	3.3	8
Weak/non-phototoxic				
Aspirin	9±2	N.D.	4.6	2
Benzocaine	N.D.	4±0	N.D.	1
Erythromycin	N.D.	5±0	4.7	3
Phenytoin	11±8	8±1	3.5	5
Sulisobenzone	N.D.	N.D.	5.4	5

N.D.: not detected.
[a] Data represent mean ± SD for three experiments.
* $P < 0.05$, significantly different from control.

The results from the IBP assay on other drugs are summarized in Table 2, and the levels of photodynamic DNA damage by tested chemicals were estimated by decreases in the level of TO intercalation. Of all the drugs tested, 15 phototoxic compounds and all the weak/non-phototoxic chemicals were found to be less photogenotoxic. However, 12 phototoxic drugs exhibited photodynamic DNA damage, which was indicative of photogenotoxic risk.

3.4. Experimental comparative study of IBP and ROS assays

Generally, photosensitizers generate ROS, such as superoxide and singlet oxygen, after exposure to UVA/B, and the ROS act as principal toxic mediators and attack biomolecules including phospholipids, proteins, and DNA [2]. Therefore, the availability of ROS data would be efficacious to realize the potential of all phototoxic reactions including photoirritation, photoallergy, and photogenotoxicity [3,8]. In the present investigation, the ROS assay was also carried out on 27 phototoxic and 5 weak/non-phototoxic drugs (Table 2). Nine phototoxic compounds, including 8-MOP, diclofenac, doxycycline, furosemide, indomethacin, nitrofurantoin, oxytetracycline, piroxicam, and tetracycline, exhibited significant ROS generation, whereas they were predicted to be non-photogenotoxic in the IBP assay. We found no clear relationship between ROS and IBP data directly. Theoretically, the ROS assay could be used to evaluate all types of phototoxic risk, although the IBP assay could be indicative of photogenotoxic potential specifically. This might partially explain the discrepancy between ROS and IBP data.

3.5. Experimental comparative study of IBP and DNA-photocleavage assays

The photogenotoxic potential of 32 model compounds was evaluated from pBR322 DNA-photocleaving activities for comparison, as well as from the newly developed IBP assay. Generally, DNA strand breaks can be readily observed by following the conversion of supercoiled pBR322 DNA (SC) to the open circular (OC) form. The DNA-photocleaving activity of ketoprofen (200 μM) was analyzed by AGE (Fig. 3A). The addition of ketoprofen to plasmid DNA did not result in DNA photocleavage in the dark; however, pBR322 DNA damage was clearly induced by ketoprofen after UVA/B irradiation. On the basis of its band intensity, there appeared to be a ca. 74% structural conversion of plasmid DNA from the SC to the OC form.

DNA-photocleaving activities of other chemicals were determined and are summarized in Table 2. No significant structural conversion of plasmid DNA was observed in negative control groups. Interestingly, not all phototoxic drugs induced photodynamic impairment of DNA. These findings were partly consistent with the results from the IBP assay, although the order of DNA damage severity observed in the AGE analysis did not completely correspond to that in the IBP assay. For further comparison, the results from the DNA-photocleavage and IPB assays were ana-